Power Decoupling Control For Grid - Forming Inverters

Master Thesis

Bendik Eikenes

Power Electronics and Drives, PED, 30-5-2024

4^{th} Semester Project

Energy
Aalborg University
http://www.aau.dk

AALBORG UNIVERSITY
STUDENT REPORT

Title:
Power Decoupling Control in Grid - Forming Converters

Project Period:
Spring Semester 2024

Project Group:
PED4-1043

Participant(s):
Bendik Eikenes

Supervisor(s):
Arman Oshnoei
Hoda Sorouri

Page Numbers:56

Date of Completion:
May 30, 2024

Abstract:

This thesis focus on decoupling active and reactive power for a grid forming(GFM) inverter using virtual impedance control. The goal is to increase the X/R ratio to 10 or more to make the feeder impedance inductive. When this is the case the phase angle and voltage magnitude controls the active and reactive power separately leading to a decoupling between the powers. When the X/R ratio is low or in other words the impedance is resistive the powers can not be controlled properly because the phase angle and voltage does not have the same relationship to the powers. This leads to instability and weak dynamic performance. The virtual impedance proposed in this project uses a negative resistance and a positive virtual impedance to increase the X/R ratio. To test the decoupling effect power steps with different X/R ratios and grid strength will be applied and the coupling and step response during the steps will be examined. The tests will be done through simulations in Simulink and on a experimental setup. From both the simulations and experimental test it can be concluded that virtual impedance had a decoupling effect for the strong grid. For the weaker grid there was a clear decoupling during the active power step. However this was not the case under a reactive power step. The virtual impedance also lead to a significant damping effect on the system.

Acronyms

GFM	Grid-Forming
GFL	Grid-Following
SG	Synchronous Generator
IBRs	Inverter Based Resources
SCR	Short Circuit Ratio
LPF	Low Pass Filter
APC	Active Power Controller
RPC	Reactive Power Controller
PCC	Point of Coupling
Pk	Peak
rms	Root Mean Square
d-axis	Direct Axis
q-axis	Quadrature axis
PI	Proportional Integral
FCS-MPC	Finite Control Set-Modular Predictive Control
THD	Total Harmonic Distortion

Nomenclature

Variables

ω_0	Nominal Angular Frequency	rad/s
ω	Angular Frequency	rad/s
C_f	Filter Capacitance	V
f	Frequency	Hz
f_0	Nominal Frequency	Hz
I_f	Filter Inductor Current	V
L_f	Filter Inductance	H
L_g	Grid Inductance	H
R_f	Filter Resistance	Ohm
R_g	Grid Resistance	Ohm
R_v	Virtual Resistance	Ohm
T_s	Sampling Time	s
V_0	Output Filter Capacitor Voltage	V
V_{abc}	abc Voltage	V
V_{nom}	Nominal Voltage	V
X_g	Grid Reactance	V
X_v	Virtual Reactance	Ohm
Z_g	Grid Impedance	H

Contents

Chapter 1

Problem Analysis

Since the beginning of the power grid, synchronous generators have been the main type of power system. Due to a large demand for renewable energy over the last years, solar and wind power systems are becoming a significant part of the grid [1]. These power systems use inverters to synchronous to the grid and are referred to as inverter based resources(IBRs). With the increase of IBRs grid instability emerge due to lack of grid supporting capabilities that synchronous generators(SG) posses. A solution to these instabilities is the inverter control method of grid-forming(GFM). This method can improve grid support by making it's own voltage reference, therefore it also works well for weak grids. Figure 1.1 shows a simplified schematic of a GFM inverter.

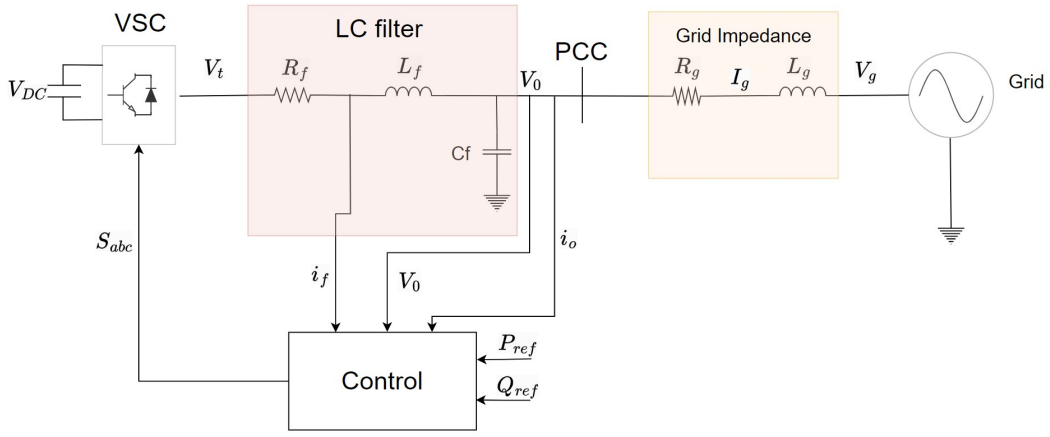

Figure 1.1: Schematic of simplified GFM inverter.

The control block contains power controllers and usually an inner loop to regulate voltage. GFM control typically uses droop control to control the power. This method controls the active power by the adjusting the frequency and reac-

tive power by controlling the voltage magnitude. However droop control needs a inductive feeder impedance to work properly. This is not the case for low voltage grids where the line is more resistive, this can be seen in Figure 1.2 [2].

Type of line	R (Ω/km)	X (Ω/km)
Low-voltage line	0.642	0.083
Medium-voltage line	0.161	0.190
High-voltage line	0.06	0.191

Figure 1.2: Line resistance and reactance per kilometer[2].

When the feeder impedance is resistive the active and reactive power cannot be controlled separately by droop control, leading to significant coupling between the two powers [3]. This results in instability and weak transient response in the system. To decouple the powers virtual impedance control can be used. The goal of this method is to increase X/R ratio of the feeder impedance to make it inductive. The X/R ratio is the line reactance divided by the line resistance. When this ratio is above 10 the line should be inductive, thus decoupling the active and reactive power.

1.1 Grid Connected Inverter Control

This section will look into the difference between conventional GFL inverters and GFM inverters and how the function. Also the power and virtual impedance control GFM inverter will be introduced.

1.1.1 GFL and GFM

The main goal of grid connected inverters is to supply the grid with active and reactive power [1]. GFL usually focus mainly on supplying the grid with active power, the reactive power is usually kept at zero or as low as possible. GFL is required to have some grid support but it is limited as it works as current source and it's reference comes from the grid. This means that if the grid is weak, changes in the grid will give a worst reference leading to instability. GFM however creates a voltage and frequency reference that can inject active power into the grid during stable operation and the needed reactive power needed to stabilize the grid when needed. These capabilities give characteristics of an SG. These characteristics include blank start capabilities, virtual inertia, better over-current regulations and better frequency support during grid changes [4]. This makes GFM a better alternative for isolated and weak grids and when stability is needed in a grid. GFL is however better at current regulations as it is a current source. Figure 1.3 shows

a simplified representation of the GFL and GFM inverters, GFL is a current source with a highly inductive impedance in series and GFM is a voltage source with a low impedance in series [2].

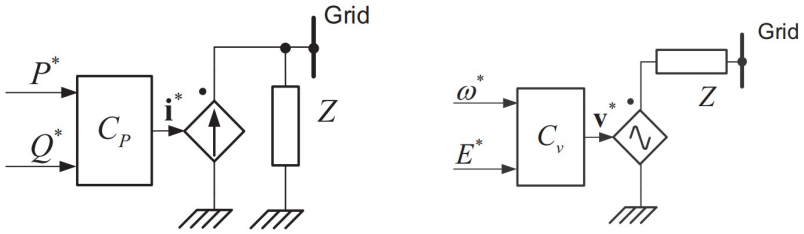

(a) GFL **(b)** GFM

Figure 1.3: Simplified representation of GFL and GFM. [2]

The Cp and Cv blocks in 1.3 are the control parts needed to get the references. As seen GFL uses the active and reactive power to calculate the current reference while GFM creates its own angle and voltage reference. GFL uses a phase-locked loop(PLL) method to synchronize with the grid [2] More information about the PLL is found in Appendix A.

1.1.2 GFM Power Control

The goal of GFM power control is accurate active and reactive power control. The conventional droop control method is a well established method and is frequently used to control the active and reactive power separately [1]. The power exchange between the inverter and grid can be shown by the following two equations[3].

$$P_g = \frac{V_0 V_g}{Z_g} cos(\theta - \delta) - \frac{V_g^2}{Zg} cos(\theta) \tag{1.1}$$

$$Q_g = \frac{V_0 V_g}{Z_g} sin(\theta - \delta) - \frac{V_g^2}{Zg} sin(\theta) \tag{1.2}$$

where V_0 and V_g is the instantaneous rms output voltages of the GFM inverter and grid side respectively. δ is the phase angle between the grid and inverter. $Z_g \angle \theta$ is the line impedance where θ is the power factor angle between the grid voltage and current. For droop control to function the line impedance needs to be inductive. At $Z_g \angle 90$ the grid is purely inductive and if δ is small the power equations can be simplified to:

$$P_g \approx \frac{V_0 V_g}{X_g} \delta \tag{1.3}$$

$$Q_g \approx \frac{V_0}{X_g}(V_0 - V_g) \tag{1.4}$$

Here X_g is the line reactance. Equation 1.3 shows the relationship between the phase angle δ and the active power. The frequency of the output voltage can alter the phase angle which gives the following relationship.

$$\omega - \omega_o = -K_{p,apc}(P - P_0) \tag{1.5}$$

Where ω_0 and ω is the reference frequency and output voltage frequency respectively. P is the measured output active power and P_0 is the reference active power. $K_{p,apc}$ is the droop gain acting like a proportional gain for the active power control. To control the reactive power the magnitude of the inverter output power can be controlled giving the following equation.

$$V - V_0 = -K_{p,rpc}(Q - Q_0) \tag{1.6}$$

Here Q are the output reactive power and Q_0 is the reference reactive power respectively. $K_{p,rpc}$ is the droop gain which also works as the proportional gain for the reactive power control. The droop gains are found by the following equations[5]:

$$K_{p,apc} = \frac{\Delta\omega}{P_{max}} \tag{1.7}$$

$$K_{p,rpc} = \frac{\Delta V}{Q_{max}} \tag{1.8}$$

Here $\Delta\omega$ is the difference between the reference frequency and maximum frequency limit. P_{max} is the maximum active power capacity. ΔV the difference between the reference voltage and maximum voltage limit. Q_{max} is the maximum reactive power capacity.

1.1.3 Virtual Impedance Control

As mentioned the conventional droop control method needs an inductive feeder impedance. To make a resistive grid have an inductive feeder impedance virtual impedance can be added [3]. This method adds the effect of a positive virtual reactance and a negative resistance to the voltage reference. The virtual reactance gives the effect of an inductor in series between the inverter and point of coupling(PCC). The added virtual impedance should give a X/R ratio larger than 10. This will decouple the active and reactive power. The equation below shows the effect of the line and virtual impedance on the voltage reference[6].

$$V_0\angle\delta v = (R_g + R_v + jX_g + jX_v)I_g\angle\theta \tag{1.9}$$

R_g and R_v is the grid and virtual resistance and Z_g and Z_v is the grid and virtual reactance.

Figure 1.4 shows an equivalent model of the GFM inverter with the virtual resistance[4].

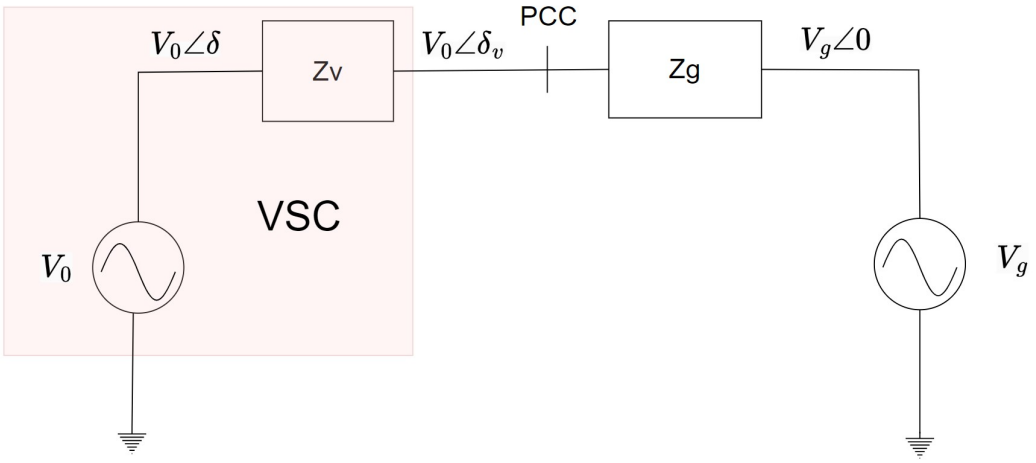

Figure 1.4: Equivalent model of GFM inverter with virtual impedance[4].

Here $V_0\angle\delta$ and $V_0\angle\delta_v$ is the output voltage without and without the virtual impedance respectively. $V_g\angle0$ is the grid voltage. Z_g and Z_g is the grid and virtual impedance respectively.

1.1.4 Grid Strength

The stronger the grid the better the voltage will be preserve or fixed during disturbances and in steady state operation [7]. The grid strength is determined by the the short circuit ratio(SCR) which is determined by the grid impedance, voltage magnitude and rated apparent power as seen in the following equation [8]:

$$SCR = \frac{1.5V_g^2}{S_n Z_g} \tag{1.10}$$

Here V_g is the ground to phase grid rms voltage, S_a is the rated apparent power and Z_g is the grid impedance. When the SCR is above 3 the grid is strong and when it is under 2 it is very weak. For remote low voltage micro-grids the long transmission lines leads to a weak grid. When the SCR is above 3 the grid is strong and when it is under 2 it is very weak.

1.2 Research Question

"Will virtual impedance decouple the active and reactive power for a resistive grid?"

1. How will different X/R ratios effect the power coupling and dynamic behavior during power steps?
2. How does the grid strength effect power coupling and dynamic behavior for different X/R ratios?

1.2.1 Technical objective

The objectives for this project are listed below.

- Explain the operational principals of inner and outer loops and virtual impedance control.
- Design active and reactive power controllers using PI controllers, inner loop control with FCS-MPC and virtual impedance control for the system.
- Evaluate the decoupling effect and dynamic behaviour of the active and reactive power by making simulations in Simulink with three different X/R ratios. These ratios will be tested with a strong and a weaker grid.
- Conduct experimental test on an experimental set-up for a GFM inverter according to the schematic in Figure 2.1. This was done by dSpace 1202 which is the prototyping system executing the control systems.

Chapter 2

Modeling

This chapter focus on theory and design of the GFM inverter used in this project. The GFM inverter includes an inner loop that uses finite control set-modular predictive control(FCS-MPC), the active power control(APC), reactive power control(RPC) and virtual impedance control. Figure 2.1 shows the grid connected GFM inverter with the controllers mentioned.

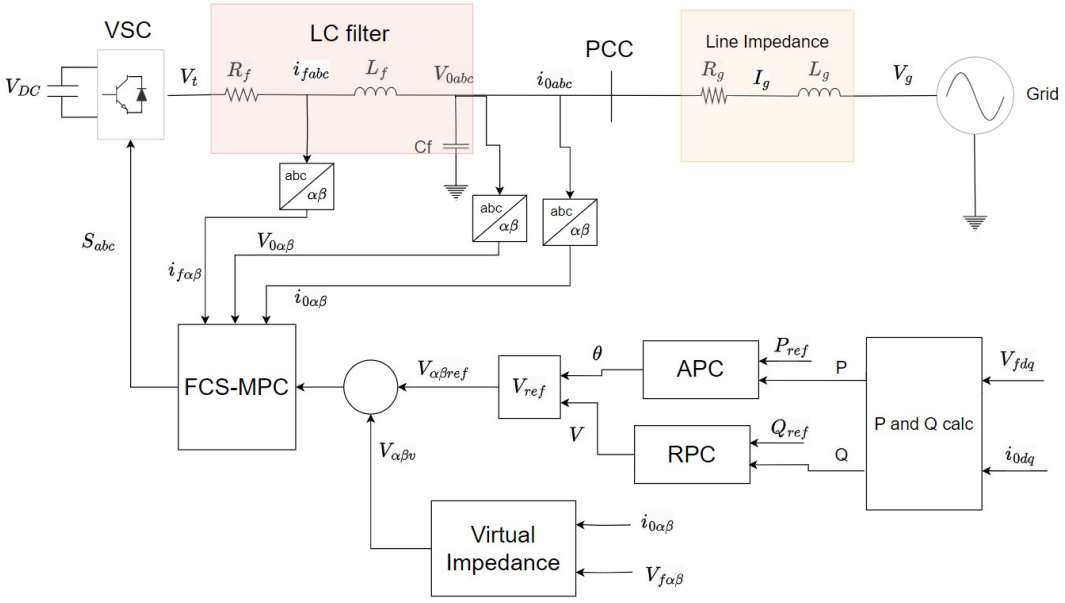

Figure 2.1: Schematic of GFM control with virtual impedance.

The VSC is a 2-level 3-phase voltage source inverter. The inner loop uses feedback from the LC filter voltage and current, and current from the point of coupling(PCC) to regulate the voltage [9]. The voltage and current feedback un-

dergo reference frame transformation to give the correct reference frame. The grid impedance is represented by a resistor and inductor in series. The LC filter is used to remove unwanted harmonics from the output voltage. The resistive part of the LC filter is a small resistance included in the filter. Table 2.1 shows the grid and filter parameters, the parameters with 2 values is for the strong grid(SCR of 13) to the left and the weaker grid(SCR of 3) to the right.

Table 2.1: System parameters for the simulation.

Parameter	Symbol	Value
Grid Voltage Phase-to-Ground	V_g	70 Vrms
Nominal Grid Frequency	f_0	50 Hz
Sampling Time	T_s	20 μs
Grid Strength	SCR	13/3
Grid Resistance	Ω	.4/1 Ω
Grid Inductance	L_g	3.6/15.5 mH
Grid Reactance	X_g	1.13/4.87 Ω
Filter Inductance	L_f	2.4 mH
Filter Capacitance	C_F	15 μF
Resistance in LC filter	R_f	0.1 Ω
Filter Cutoff frequency	kHz	2.5

Here it grid voltage is 70 Vrms which is the case for the simulation tests. For the experiments however this voltage was 35 Vrms because a higher voltage cause faults in the system.

2.1 Inner Loop Control

The inner control loop is used for voltage regulation [9]. The conventional method employs a dual loop topology with PI controllers. Having a dual loop topology often leads to bandwidth problems which leads leads to weaker dynamic performance. Also dual inner loop control leads to worst robustness during parameter changes and the lack the ability of balancing the various control intentions effectively [10]. An alternative method to deal with these problems is finite control set-model predictive control(FCS-MPC). This method can handle multiple inputs and determine the optimal action for the next step or multiple steps for the best performance.

2.1.1 Finite Control Set-Model Predictive Control

In this project the FCS-MPC method was utilized to determine the next optimal switching state for the inverter for each time step. For inverters, it can however be

relevant to predict multiple steps ahead when switching at lower frequencies [10]. The inverter employed in this project is a two-level, three phase inverter with eight different switching states, as shown in Figure 2.2.

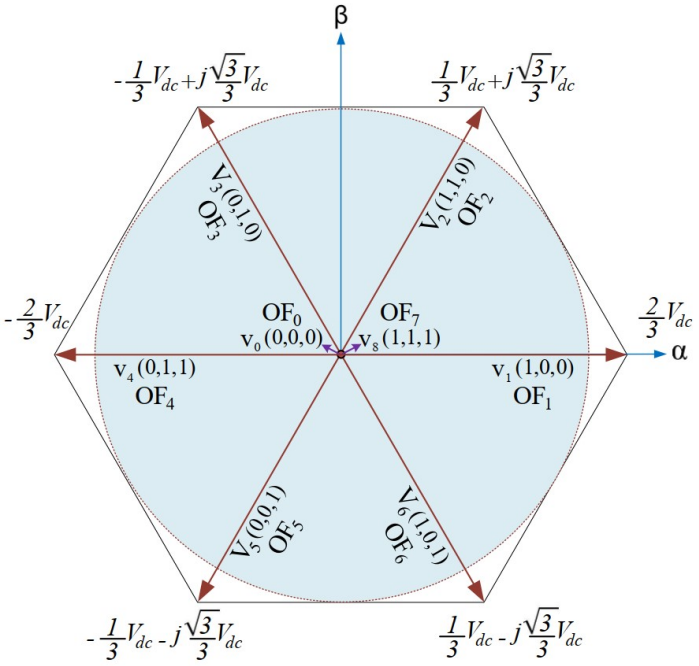

Figure 2.2: The voltage vectors that the inverter can apply[9].

Keep in mind that OF_0 and OF_7 reach the same value, but use different switches.

FCS-MPC implements all the switching states into the discrete model of the inverter to predict the output current and voltage. These values will then be implemented into a cost function to decide which switching state to use. The differential equation for the LC filter as shown in the following equation.

$$L_f \frac{di_f}{dt} = V_i + V_0 + R_f i_f \tag{2.1}$$

$$C_f \frac{dv_f}{dt} = i_f - i_0 \tag{2.2}$$

Here C_f and L_f is the LC filter capacitance and inductance respectively. i_f is the inductor current and V_0 is the capacitance voltage. V_i is the voltage vector state of the inverter and i_0 is the output current. These differential equations give the following continuous state space model.

$$\frac{d}{dt}\begin{bmatrix} i_f \\ V_0 \end{bmatrix} = \begin{bmatrix} -\frac{Rf}{L_f} & -\frac{1}{L_f} \\ \frac{1}{C_f} & 0 \end{bmatrix}\begin{bmatrix} i_f \\ V_0 \end{bmatrix} + \begin{bmatrix} \frac{1}{L_f} & 0 \\ 0 & -\frac{1}{C_f} \end{bmatrix}\begin{bmatrix} V_i \\ i_0 \end{bmatrix} \tag{2.3}$$

Zero order hold is used to make the continuous model into a discrete model. This has to be done for digital implementation. The following equation shows the discrete model equation.

$$\begin{bmatrix} i_f(k+1) \\ V_0(k+1) \end{bmatrix} = \begin{bmatrix} -\frac{Rf}{L_f} & -\frac{1}{L_f} \\ \frac{1}{C_f} & 0 \end{bmatrix}\begin{bmatrix} i_f(k) \\ V_0(k) \end{bmatrix} + \begin{bmatrix} \frac{1}{L_f} \\ 0 \end{bmatrix} V_i(k) + \begin{bmatrix} 0 \\ -\frac{1}{C_f} \end{bmatrix} \tag{2.4}$$

This equation will predict the output voltage and inductor current for the next time step. The voltages and currents measurements of the system are transferred from the abc reference frame to $\alpha\beta$ by Clark Transformation. The predicted current and voltages are then implemented into the cost function.

$$CF = (V_0^*\alpha - V_0\alpha)^2 + (V_0^*\beta - V_0\beta)^2 + \lambda_\omega SW^2 + \lambda_{der}G_{der} \tag{2.5}$$

λ_{der} and λ_ω are the weighting factors for G_{der} and SW respectively. G_{der} is used to regulate for the error from the derivative of the output voltage. SW considers the amount of transistor switching that has to be done to get into the next state, so the more switches that need to be switched the higher SW is. G_{der} is found by the following equation.

$$G_{der} = (C_f\omega^* V_0^*\alpha - i_f\alpha + i_0\alpha)^2 + (C_f\omega^* V_0^*\beta + i_f\beta - i_0\beta)^2 \tag{2.6}$$

The equation for SW:

$$SW = ||v_i(k) - v_i(k-1)|| \tag{2.7}$$

$v_i(k)$ is the switching for this step and $v_i(k-1)$ is for the previous step.

Figure 2.3 shows the block diagram of the FCS-MPC controller.

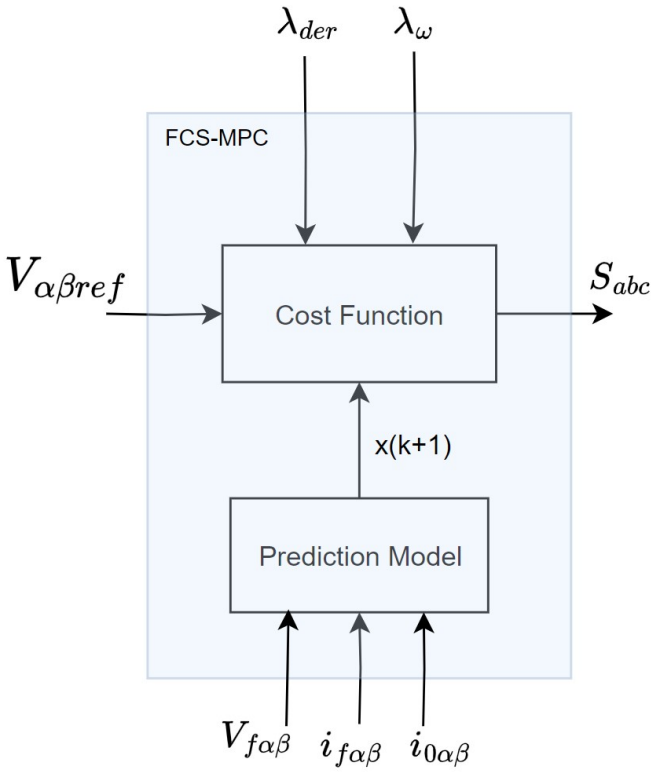

Figure 2.3: Block diagram of FCS-MPC [9].

Here S_{abc} is the switching signal that tells the inverter to switch to get the reference voltage.

Table 2.2 shows the weighting factors used in this project. These values were the ones implemented in the experimental set-up, therefore these were also used for the simulation.

Table 2.2: Weighting factors used in the project.

Parameter	Value
λ_{der}	3
λ_{ω}	1

2.2 Power Control

The power control in this project is based on conventional droop control. Both the active and reactive power control will use a PI controller where the proportional gain is determined by droop characteristics and the integral gain is implemented to get rid of the steady state error. Although the integral part of the active power

controller(APC) is not necessary, a small integral gain is added to maintain PI controllers for both the APC and RPC. As the droop equations were introduced in Chapter 1 this section will focus on the explaining the power loops, the design of the controllers and the frequency and step response of the system.

2.2.1 Active Power Control(APC)

Figure 2.4 shows the block diagram of the active power loop [1].

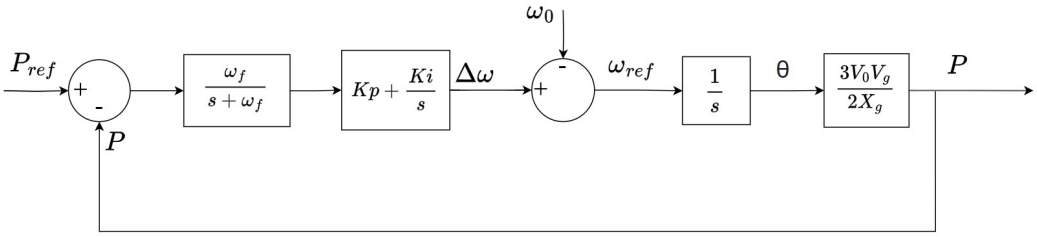

Figure 2.4: Active power control loop [1].

The PI adjusts frequency reach the active power reference. The active power error goes through the first order low pass filter with a cut-off frequency of ω_f before the PI controller. The PI then computes the change in frequency needed to correct the active power error which is added to the nominal frequency ω_0 to get the reference frequency ω. This frequency is integrated to get the power angle θ needed to correct the active power. The angle multiplied by simplified power exchange equation between inverter and grid from Equation 1.3. Although the integral part of the active power control is not necessary a small integral gain is added to have a PI controller for both controllers. Therefore for the rest of this section the bode and step response will not include the integral part.

To measure the output active power of the the inverter the following equation is used.

$$P = V_0 di_0 d + V_0 q i_0 q \tag{2.8}$$

Here the voltages and currents of the PCC are transferred to the dq domain by the park transformation.

The open loop transfer function is shown below.

$$G_{OL} = K_{p,apc} \cdot \frac{\omega_f}{s+\omega_f} \cdot \frac{1}{s} \cdot \frac{3V_0V_g}{2X_g} \tag{2.9}$$

It is assumed that V_0 and V_g are both 70 V is 10 when plotting the bode and closed loop diagrams. ω_f is 10.

The closed loop transfer function:

$$G_{CL} = \frac{G_{OL}}{1 + G_{OL}} \tag{2.10}$$

$K_{p,apc}$ was found by using Equation 1.7 from the previous chapter. The frequency variation used was 2%, this value is within the droop coefficient limit for generators in Europe which is between 2% and 12% [11]. Also from testing the different droop coefficient in the simulation and in step responses in Matlab 2% gave a good step response compared to higher values.

$$K_{p,apc} = \frac{0.02 \cdot 50}{1000} = 0.001 \tag{2.11}$$

Figure 2.5 shows the open loop bode plot for the active power loop for the strong and weaker grid using the calculated $K_{p,rpc}$ value.

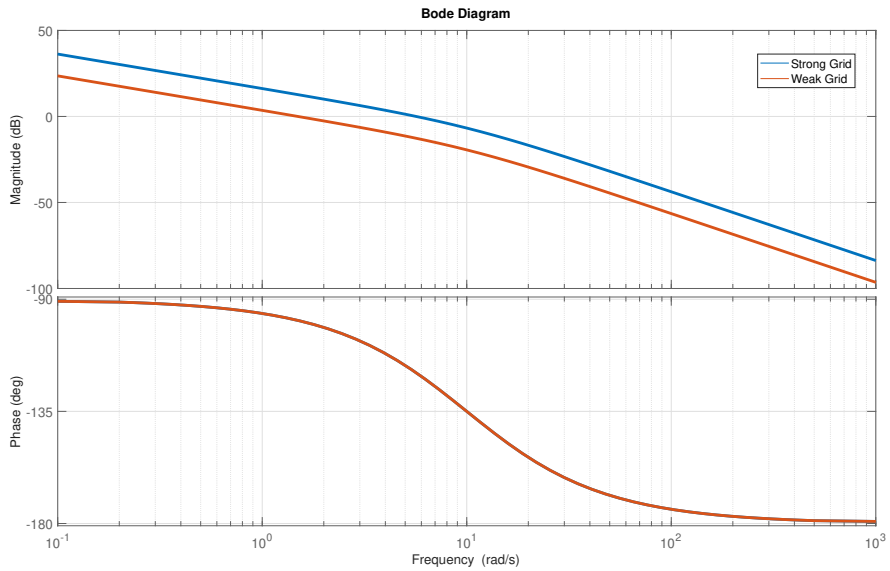

Figure 2.5: Open loop bode plot.

The table below shows the gain and phase margins of the system with a strong and weaker grid.

Table 2.3: Gain and Phase Margins for Strong and Weak Grid

Parameter	Strong Grid	Weaker Grid
Gain Margin	Infinite	Infinite
Phase Margin	60.5 degree	81.5 degree

Figure 2.6 shows the step response of the closed loop system with a strong and weaker grid.

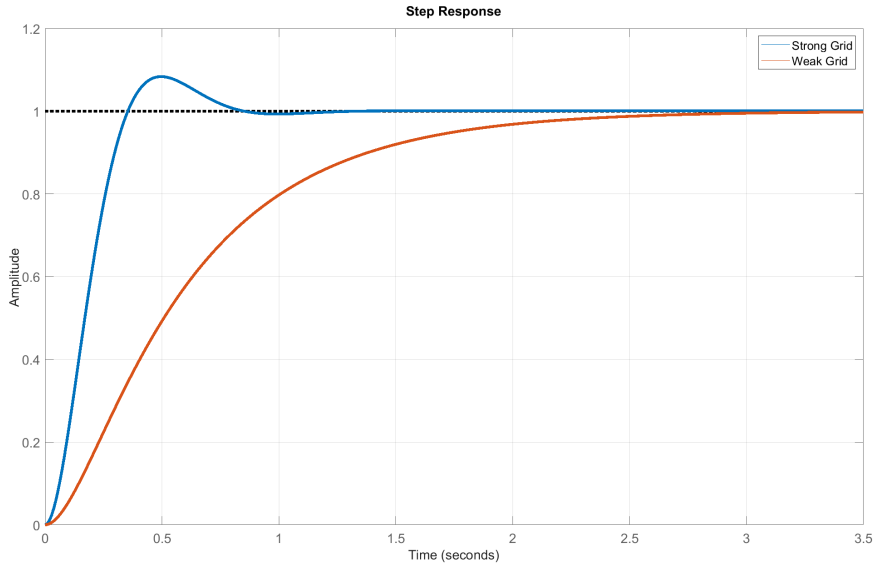

Figure 2.6: Closed loop step response.

From the gain and phase margins and step response it shows that $K_{p,rpc}$ will be a suitable gain for this system.

2.2.2 Reactive Power Control(RPC)

Figure 2.7 shows the block diagram of the reactive power loop.

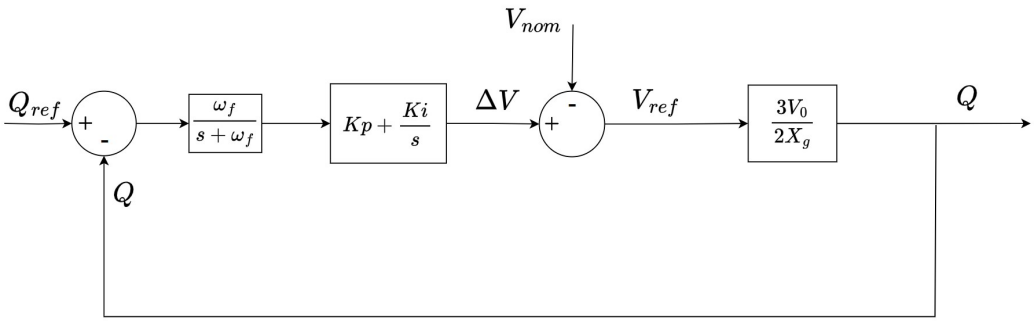

Figure 2.7: Reactive power loop.

Here the PI controller gives the needed change in voltage magnitude ΔV to reach the reactive power reference. Before the reactive power error goes to the PI controller it goes through a first order low pass filter. This correction change will be added with the nominal voltage V_{nom} to get the reference voltage V_{ref}. By multiplying the V_{ref} with $\frac{3V_0}{2X_g}$ we get Equation 1.4 which gives the reactive power flowing from the inverter to the grid. Here there is also a low pass filter in the feedback. To measure the output active power of the the inverter the following equation is used.

$$Q = V_0 q i_0 d - V_0 d i_0 q \tag{2.12}$$

Here the dq voltages and currents of the PCC are transferred to the dq domain by the park transformation.

The open loop transfer function is shown below.

$$G_{OL} = (K_{p,rpc} + \frac{K_{i,rpc}}{s}) \cdot \frac{\omega_f}{s+\omega_f} \cdot \frac{3V_0}{2X_g} \tag{2.13}$$

The closed loop transfer function is then:

$$G_{CL} = \frac{G_{OL}}{1+G_{OL}} \tag{2.14}$$

The reactive power droop gain is calculated by using Equation 1.8. The drop coefficient was 2 percent like for the APC and the maximum reactive power was

400 VAr, which was an estimated value as the maximum value was not certain. This gives the following calculation for the droop gain:

$$K_{p,rpc} = \frac{0.02 \cdot 70}{400} = 0.0035 \tag{2.15}$$

To find the integral gain the closed loop transfer function was used. The reactive power loop transfer function can be written as [3]:

$$Q = \frac{\frac{3V_0}{2X_g}(K_{p,apc}s + K_{i,rpc})(s + \omega_f)}{s^2 + 2\delta\omega_n s + \omega_n^2} Q_{ref} \tag{2.16}$$

This gave the the damping coefficient δ and natural frequency ω_n:

$$\delta = \frac{\omega_f(1 + K_{p,apc}\frac{3V_0}{2X_g})}{2\omega_n} \tag{2.17}$$

$$\omega_n = \sqrt{\frac{3V_0}{2X_g}\omega_f K_{i,rpc}} \tag{2.18}$$

The value decided for $K_{i,rpc}$ will be 0.132 as this gave a critical damping for the weaker grid and a good closed loop step response for the strong grid as seen in Figure 2.8.

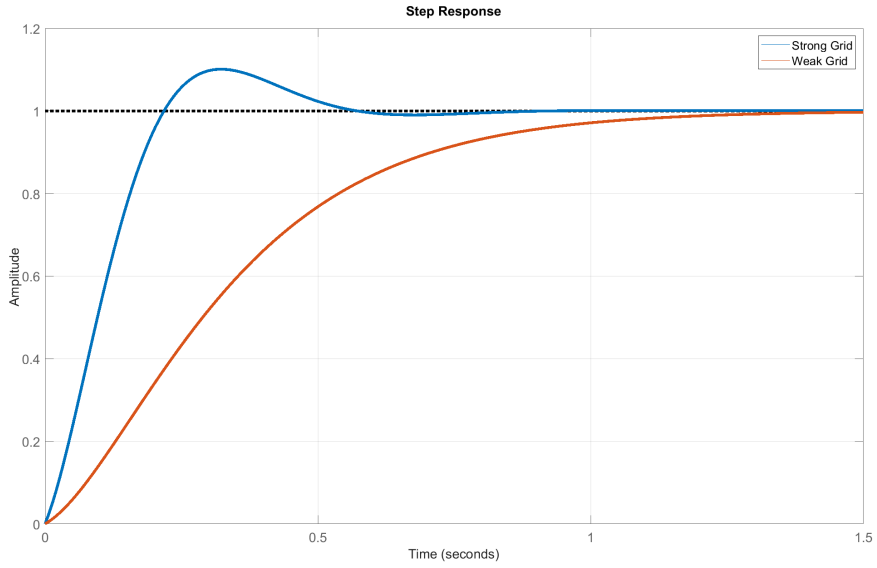

Figure 2.8: Closed loop step response for RPC loop.

Figure 2.9 shows the open loop bode plot for the reactive power loop.

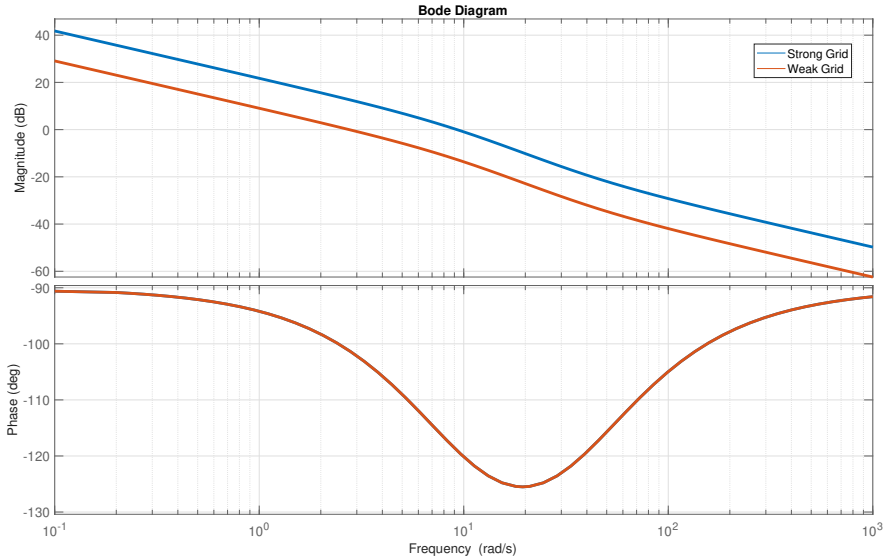

Figure 2.9: Open loop bode plot for RPC loop.

The table below shows the gain and phase margins of the system with a strong and weaker grid.

Table 2.4: Gain and phase margins for strong and weaker Grid

Parameter	Strong Grid	Weak Grid
Gain Margin	Infinite	Infinite
Phase Margin	61 degree	78.8 degree

The phase and gain margins and closed loop step response shows that the gains used gives a stable system.

2.3 Virtual Impedance Control

The virtual impedance added is determined by the virtual impedance profile(VIPR). This method calculates the virtual impedance needed to get to the desired X/R ratio. An Equivalent grid impedance estimation(EGIE) method is also implemented in this project as it can show the effect of the virtual impedance. The EGIE estimates the resistance, reactance and X/R ratio of the line impedance [3]. Figure 2.10 shows how the virtual impedance control works in this project.

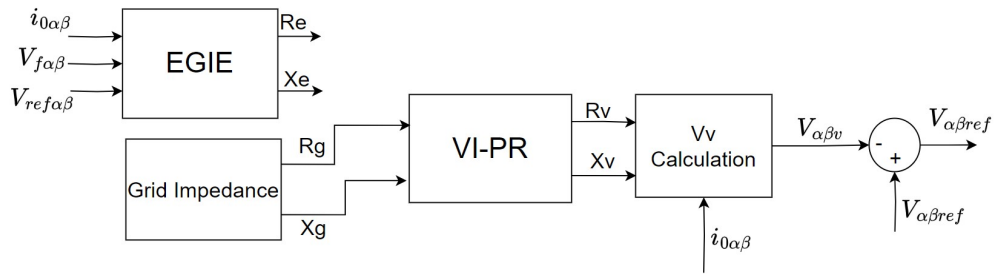

Figure 2.10: Block diagram showing how the virtual impedance is found using EGIE and VI-PR.

Here it can be seen that a voltage reference called $V_{\alpha\beta v}$ is added to the voltage vector created by the power loop to give the inverter the voltage reference. In the Figure the known grid impedance is first sent to the VI-PR block which gives the needed virtual impedance needed to decouple the power. Then a voltage reference is created by the Vv calculations to alter the feeder impedance X/R ratio. The EGIE block is there to show how it can easily be implemented to use the estimated impedance as the feed for the VI-PR.

The Vv calculations is shown below.

$$V\alpha\beta v = (Rv + Xv)i_{\alpha\beta} \tag{2.19}$$

VI-PR is one of two main virtual impedance methods. Another known method is the Q-V modified droop control(QV-MDC).This method uses voltage restoration to decouple the power. Both the mentioned methods can be used for open and closed loop control. In this project an open loop method is used as it has a fixed virtual impedance. A closed loop method would be beneficial for grids with altering impedance. Here the EGIE for example can estimate the grid impedance continuously so the virtual impedance alters to fulfill the desired X/R ratio at different grid impedance.

2.3.1 VI-PR

To determine the virtual resistance desired the grid resistance R_e is multiplied by ϕ.

$$R_v = \phi R_e \tag{2.20}$$

ϕ is gives the value needed to be multiplied to get the X/R ratio wanted, it is also depended on the power ability of the inverter This value is often negative to increase the X/R ratio. This is also the case for λ which is the value needed to get the desired virtual impedance seen in the equation below. This equation gives the desired virtual reactance.

$$X_v = \lambda X_e \tag{2.21}$$

2.3.2 EGIE

To estimate the grid impedance EGIE calculates the overall power that includes the effect of the virtual impedance [3]. This effect is not included in the active and reactive power equations 2.8 and 2.12. The following equation shows the overall power equations used:

$$P_c = \delta v_{c\alpha} i_{o\alpha} + \delta v_{c\beta} i_{o\beta} \tag{2.22}$$

$$Q_c = \delta v_{c\beta} i_{o\alpha} - \delta v_{c\alpha} i_{o\beta} \tag{2.23}$$

Here $\delta V_{c\alpha} = V^*_{f\alpha\beta} - V_{f\alpha\beta}$ is the difference between the reference and output inverter voltage. $i_{0\alpha\beta}$ is the measured PCC current.

The impedance can be estimated by:

$$Z_e = \frac{V^*_\alpha}{i_{o\alpha}} = \frac{V^*_\beta}{i_{o\beta}} \tag{2.24}$$

Here $V^*_{f\alpha\beta}$ and $i_{0\alpha\beta}$ is the rms reference voltage and rms PCC current respectively. The equations below is then used to estimated the resistance and impedance of the grid.

$$r_e = \frac{Z_e P_c}{S_c} \tag{2.25}$$

$$x_e = \frac{Z_e Q_c}{S_c} \tag{2.26}$$

Here S_c is the apparent power of the system with the virtual impedance added.

$$S_c = \sqrt{P_c^2 + Q_c^2} \tag{2.27}$$

There is a maximum reactance limit that can be added to the inverter because of it's power limit.

$$x_{max} = \frac{3V_g^2}{\sqrt{S_r^2 - P_g^2}} \tag{2.28}$$

Here V_g is the rms nominal grid voltage, S_r and P_g is the apparent power limit and active power delivery of the inverter. The maximum active power delivery tested

in this project was 500 W and the the nominal apparent power is 1000 VA. The rms nominal rms grid voltage is 70 V, this gives the following x_{max}.

$$x_{max} = \frac{3 \cdot 70^2}{\sqrt{1000^2 - 500^2}} = 17\Omega \tag{2.29}$$

2.4 Initial Synchronization

The initial synchronization for grid inverter needs a PLL. After synchronization GFM will be used. Figure 2.11 shows the block diagram of the transition.

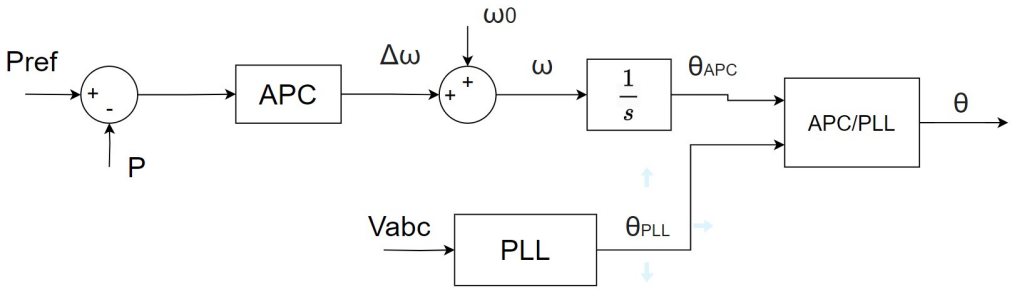

Figure 2.11: Block diagram showing PLL/APC transition.

The transition is done after a short time, in this project it will be done after 0.45 seconds. Figure 2.12 shows the transition from PLL to APC for the phase angle after around 0.35 seconds.

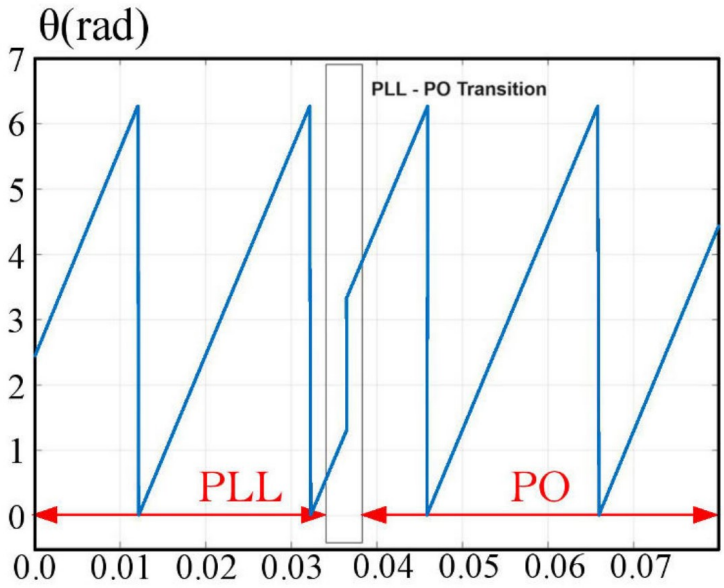

Figure 2.12: Voltage angle during PLL to APC transition.

Here PO is when the inverter operates in GFM mode.

Chapter 3

Simulation Tests

In this chapter, simulation results from the Simulink tests will be presented. The tests in this chapter will examine the coupling between active and reactive power during steps and see if increasing the X/R ratio will give less coupling. For determining the coupling effect the deviation from the reference during a step of the opposite power type will be used. Also the settling time and overshoot of the active and reactive power will be examined for the different X/R ratios. There will be 3 different X/R ratios tested for both a strong grid with a SCR of 13 and a weaker grid with a SCR of 3. The estimated resistance, reactance and X/R ratio will also be presented to show effect of the implemented virtual impedance. Voltage analysis is also implemented to make sure it is within standard THD grid requirement. According to IEEE Standard for voltage under 1 kV the THD should be under 8% and no single harmonics should be above 5% [12]. The different steps of the simulation are shown in the Table 3.1.

Table 3.1: The steps for the simulation test.

Time(s)	Step	**Active Power(W)**	**Reactive Power(VAr)**
0	PLL Synchronisation	0	0
0.45	GFL to GMF Transition	0	0
0.6	Active Power Ramp Up	0-100	0
1	Reactive Power Step	0	0-100
2	Add Virtual Reactance	0	0
3	Add Virtual Resistance	0	0
5	Active Power Step	100-800	0
8	Reactive Power Step	0	100-400

The plots for the tests exclude the start up phase as it is not relevant for the decoupling analysis. The plots will start after 4 seconds.

Table 3.2 shows the PI gains for the active and reactive controllers. Here the

gains were not the exact same as the ones in the modelling chapter as after doing multiple tests it was found that modification could be done for better responses. So more aggressive gains were used so the response would not be too slow for the weaker grid.

Table 3.2: Simulation PI controller gains for active and reactive controllers .

Parameter	Value
$K_{p,apc}$	0.0012
$K_{i,apc}$	0.00001
$K_{p,rpc}$	0.0035
$K_{i,rpc}$	0.2

Here apc and rpc stands for the is active power controller and reactive power controller respectively.

3.1 Tests on a Strong Grid

In this section the tests with different X/R ratios are presented with SCR of 13. The grid parameters of the strong grid are presented in Table 3.3.

Table 3.3: Grid line impedance and grid strength for the strong grid test.

Parameter	Value
Grid Resistance	0.4 Ω
Grid Inductance	3.6 mH
Grid Reactance	1.13Ω
X/R Grid	2.83
SCR Grid	13

The virtual impedance added and reference X/R ratios for the different tests can be seen in Table 3.4.

Table 3.4: Virtual impedance added for the tests.

Test	Virtual Resistance(Ω)	Virtual Inductive Reactance(Ω)	Desired X/R ratio
1	0	0	2.83
2	-0.2	1	10.65
3	-0.2	1.87	15

3.1.1 Test 1

In this test, no virtual impedance is added. This results in a X/R ratio of 2.83 as the grid resistance is 0.4 Ω and grid reactance is 1.13 Ω, which is inductive. Figure 3.1 shows the active and reactive power delivered to the grid during the test.

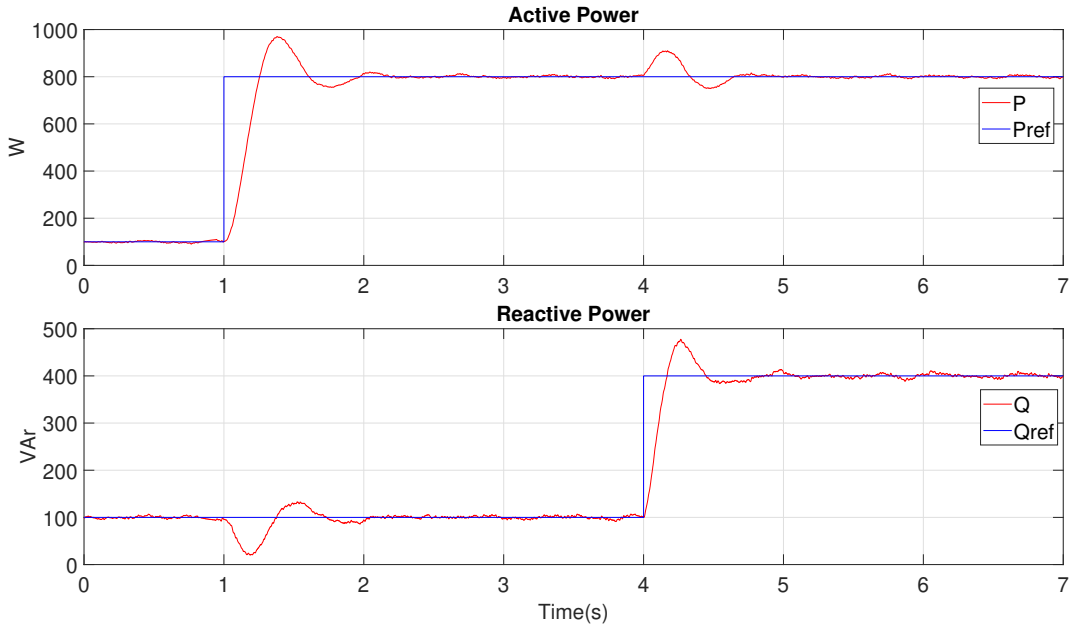

Figure 3.1: Active and Reactive Power Steps Test 1.

Here there is a clear coupling between the active and reactive power. The reactive power deviates 79.8 VAr from the reference during the active power step. The reactive power step leads to the active power deviating 110.3 W from the reference. There is a considerable overshoot of 21.3 % for the active power and 19.4% for the reactive power. The settling time is 0.9 and 1 seconds for the active and reactive power respectively. The considerable overshoot can stem from the low X/R ratio and aggressive gains needed so the weak grid test would get an acceptable transient response. The overshoot can lead some extra deviation as it went to higher active power values.

Figure 3.2 shows the estimated resistance, reactance and X/R ratio respectively during the test.

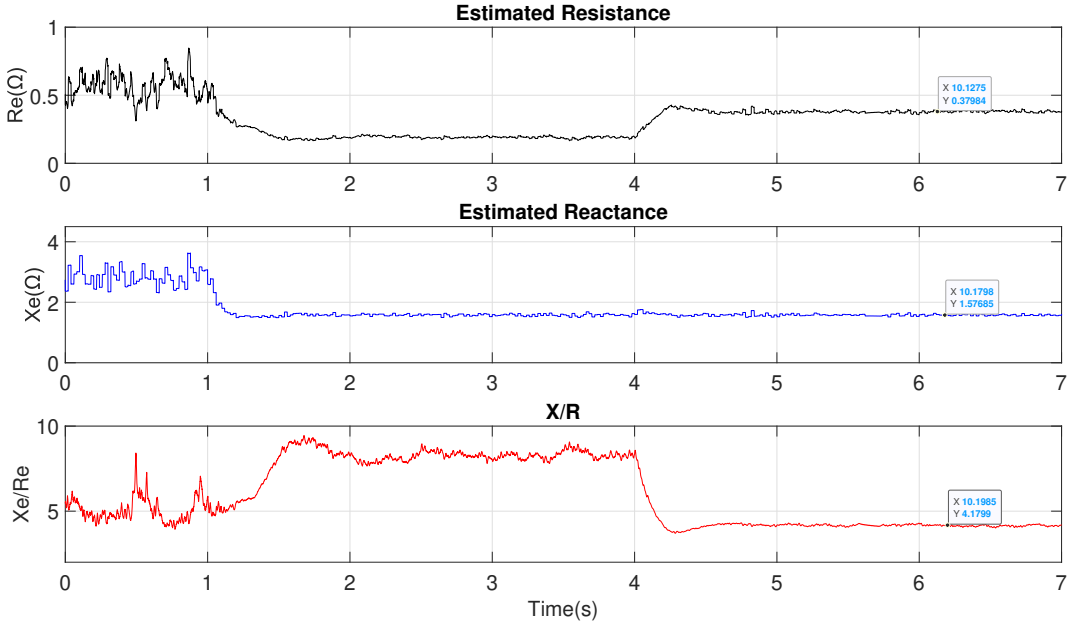

Figure 3.2: The estimated resistance, estimated reactance and estimated X/R ratio for test 1.

The estimated X/R ratio can be seen to be almost 10 before the reactive power step as the estimated resistance goes closer to zero. After the reactive power step the resistance increase and X/R goes to around 4.2. This means that the EGIE does not estimate the values with high accuracy especially not before the reactive power step.

Figure 3.3 shows the steady state abc voltage after both of the power steps have been applied.

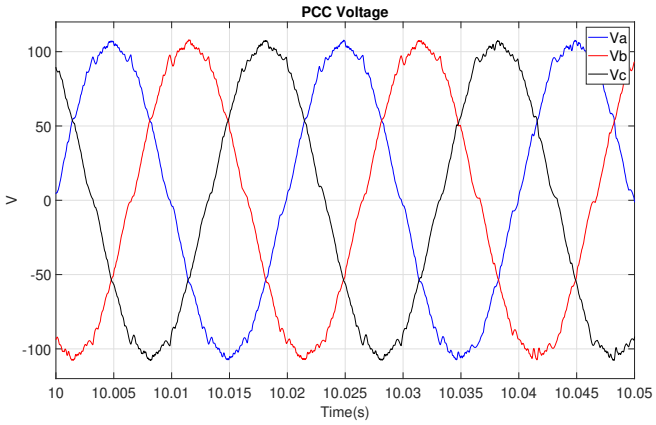

Figure 3.3: Steady state abc voltages after power steps.

Here the THD is 3.3% so it is well within the grid codes. The peak voltage here is about 108 V.

3.1.2 Test 2

This test will add a negative virtual resistance of 0.2Ω and a virtual reactance of 1Ω. This gives a X/R reference of 10.65, with the incentive of making feeder impedance inductive. Figure 3.4 shows the active and reactive power delivered to the grid during the test.

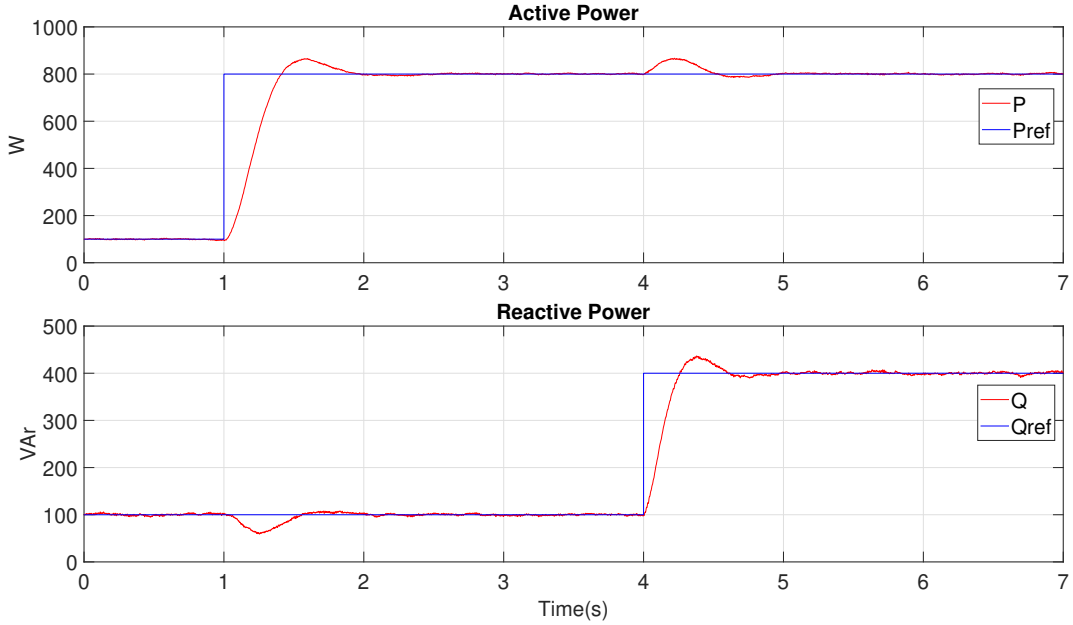

Figure 3.4: Active and Reactive Power Steps Test 2.

The coupling effect here is less than in Test 1, here the reactive power deviation is 41.1 VAr and the active power deviates 67.2 W. The settling time is shorter for both the active and reactive power step and the overshoot is considerably smaller with 8.25% for the active power and 9.25% for the reactive power. This means that the virtual impedance gives a damping effect on the systems. The smaller overshoot will effect the coupling deviation magnitude however it is clear that adding the virtual impedance leads to a decoupling effect of the powers.

Figure 3.5 shows the estimated resistance, reactance and X/R ratio respectively during the test.

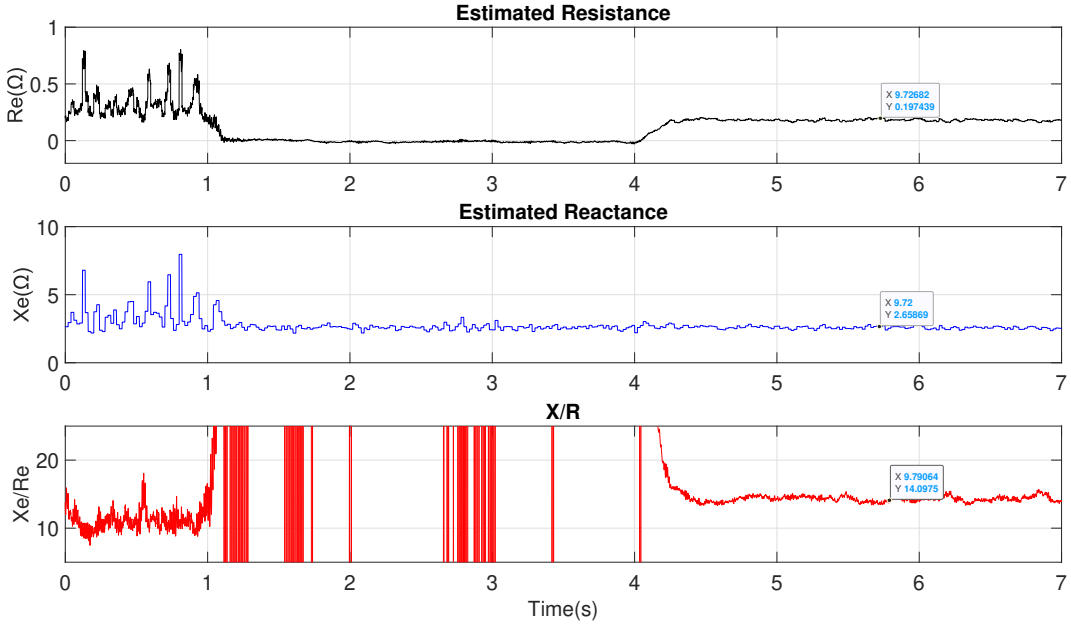

Figure 3.5: The estimated resistance, estimated reactance and estimated X/R ratio for test 2.

Here the estimated resistance goes to around zero after the active power step. This lead to a large spike in X/R ratio, which had to be cut out because of it's magnitude. After the reactive power step the resistance increase to around the reference of 0.2 Ω. The estimated reactance stays steady at around 2.65 Ω which is a bit higher than 2.13 which is the reference. This gives an estimated X/R ratio of around 14.1.

Figure 3.6 shows the steady state abc voltage after both of the power steps have been applied.

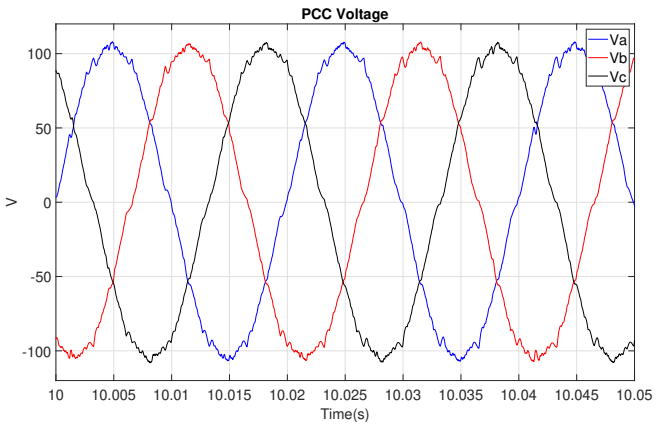

Figure 3.6: Steady state abc voltages after power steps.

Here the is THD = 3.5% so not any significant difference compared to test 1.

3.1.3 Test 3

This test will add a negative virtual resistance of 0.2Ω and a virtual reactance of 1.87Ω. This gives a X/R reference of 15. This test was done to see if a higher X/R ratio making the feeder impedance more inductive would lead to better power decoupling. Figure 3.7 shows the active and reactive power delivered to the grid during the test.

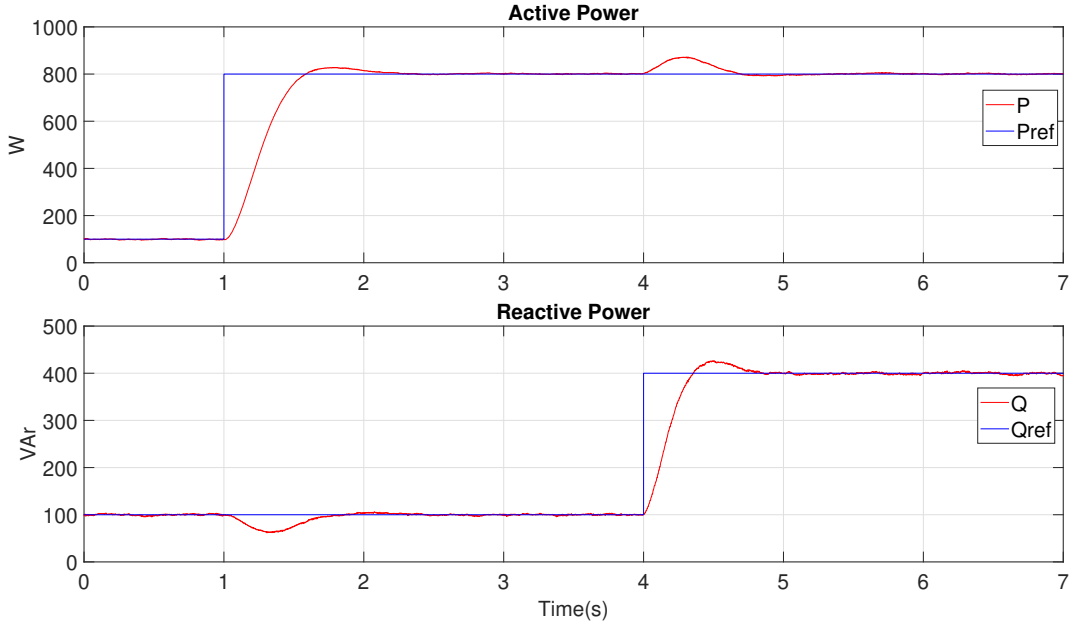

Figure 3.7: Active and Reactive Power Steps Test 3.

Here the reactive deviation was smaller than in test 2 with 38 VAr but the settling time was a slightly longer. For the active power deviation it was larger than in test 2 with 72.8 W. The active power overshoot was 3.5% and the settling time was a bit slower than the other tests with 0.96 seconds. For the reactive power the overshoot was 6.6% and the settling times was 0.78 so a bit slower than for test 2 but faster than test 1.

Figure 3.8 shows the estimated resistance, reactance and X/R ratio respectively during the test.

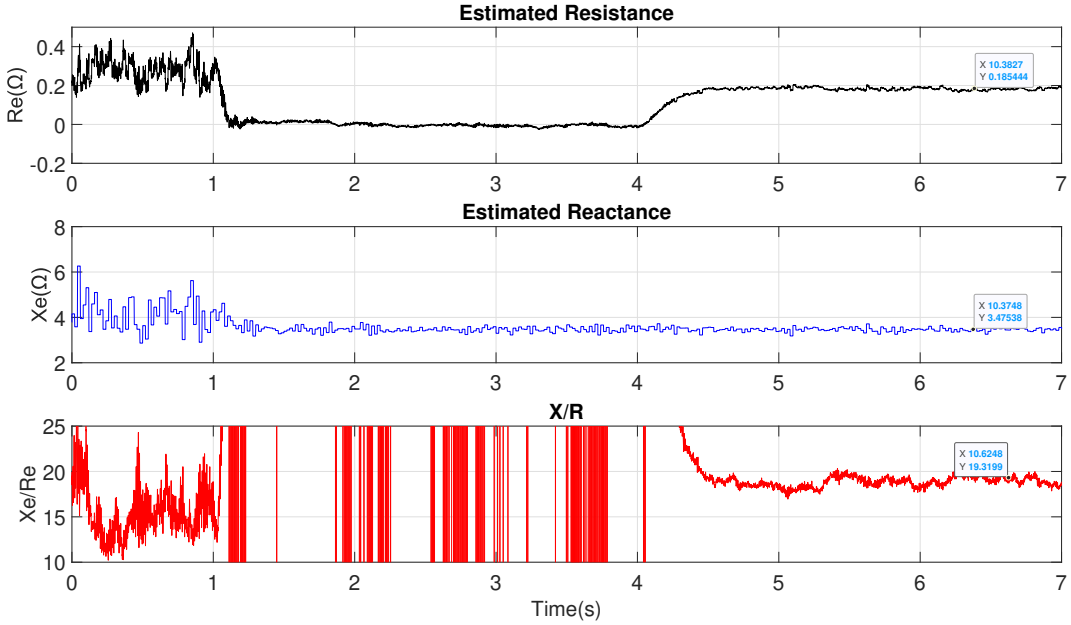

Figure 3.8: The estimated resistance, estimated reactance and estimated X/R ratio for test 3.

The estimated resistance like in test 2 goes down to around zero after the active power step giving very high X/R ratios. After the reactive power step the resistance increase to the reference of 0.2 Ω. The estimated reactance is around 3.4 Ω compared to the reference of 3. This gives an estimated X/R ratio of around 19.

Figure 3.9 shows the steady state abc voltage after both of the power steps have been applied.

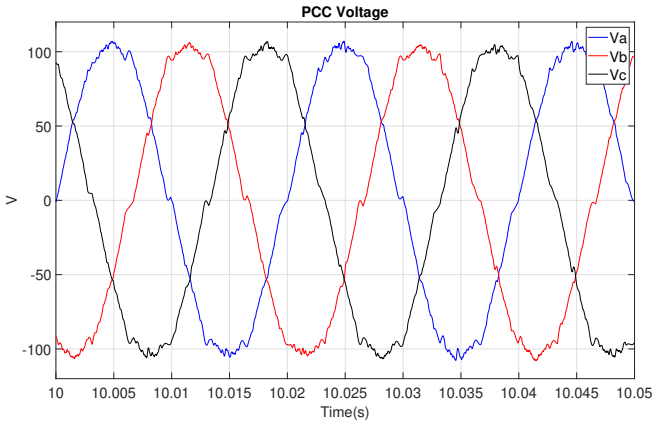

Figure 3.9: Steady state abc voltages after power steps.

Here the is THD 4% which is the largest for the strong grid tests.

3.2 Tests on a Weaker Grid

In this section the the tests with the same X/R ratios are done with a weaker grid which has a SCR of 3. This grid strength is at the limit between strong and weak. Table 3.5 shows the grid parameters.

Table 3.5: Grid parameter of weak grid.

Parameter	Value
Grid Resistance	1 Ω
Grid Inductance	15.5 mH
Grid Reactance	4.87 Ω
X/R Grid	4.87
SCR Grid	3

The grid inductance here is increased compared to test 1 to get a weaker grid and the grid resistance is increased so the virtual impedance needed to be added did not have to be too large.

The implemented virtual impedance here are added to get the same X/R ratios as the strong grid tests. Table 3.6 shows the implemented virtual impedance in the tests.

Table 3.6: Virtual impedance implemented for the weak grid tests.

Test	Virtual Resistance(Ω)	Virtual Inductive Reactance(Ω)	X/R ratio
1	0.72	0	2.83
2	-0.25	3	10.5
3	-0.4	4.15	15

3.2.1 Test 1

In this test the X/R reference is 2.83. As the X/R ratio of the grid is 4.87 a positive reactance of 0.72 Ω is added. Figure 3.10shows the active and reactive power delivered to the grid during the test.

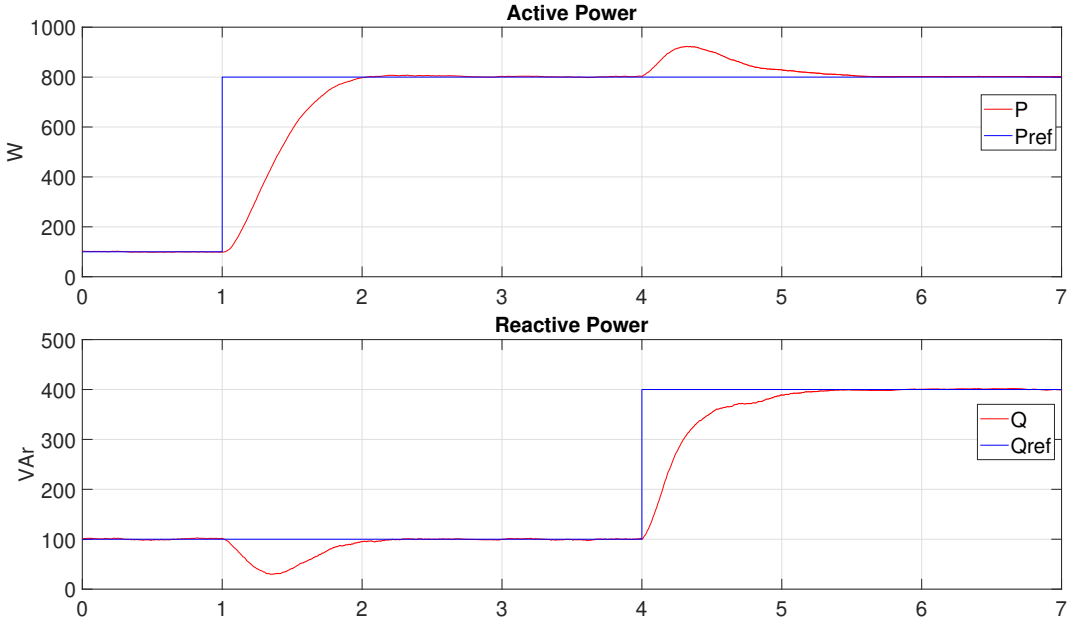

Figure 3.10: Active and Reactive Power Steps Test 1.

Here the reactive deviation is 70 VAr which is a bit smaller than for same X/R ratio with the stronger grid. However here the active power only had a 1% overshoot. The active power deviation is 123 W which is larger than for the strong grid and here the overshoot is 0% compared to 19.4 for the strong grid. The settling time for the active power is 0.92 seconds and for the reactive power it is 1.07 seconds. This is similar to the settling times of test 1 with a strong grid even though the overshoot it much larger for the strong grid, which stated earlier can lead to more deviation.

Figure 3.11 shows the estimated resistance, reactance and X/R ratio respectively during the test.

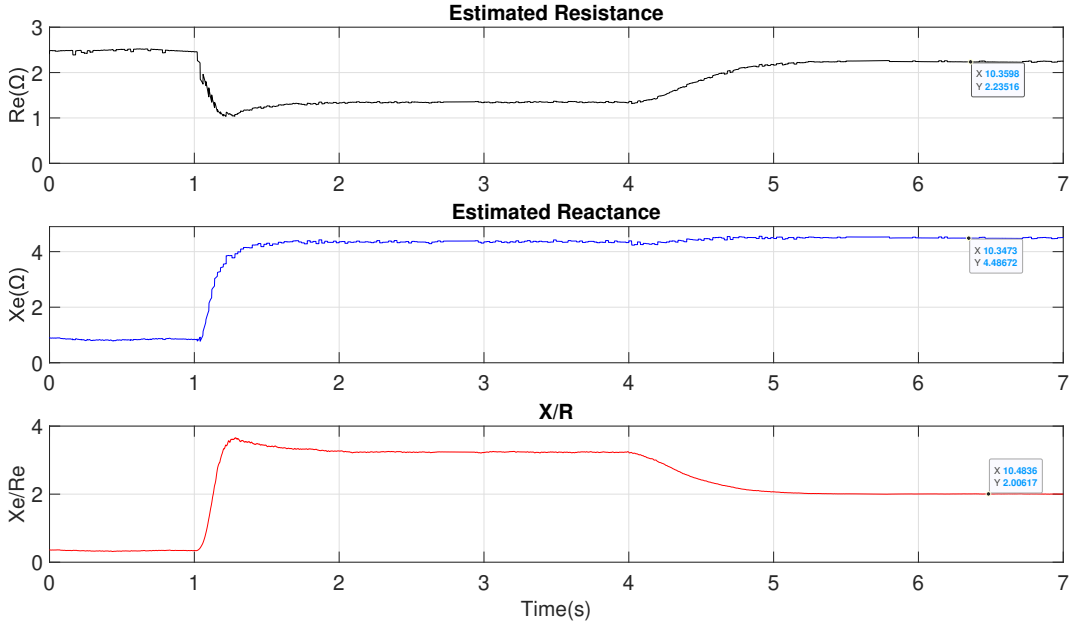

Figure 3.11: The estimated resistance, estimated reactance and estimated X/R ratio for test 1.

Here the estimated X/R is lower than the reference at about 2. The estimated resistance is around 2.2Ω which is higher than the reference of 1.72Ω. The estimated reactance is about 4.48Ω which is not far of the reference of 4.87Ω.

Figure 3.12 shows the steady state abc voltage after both of the power steps have been applied.

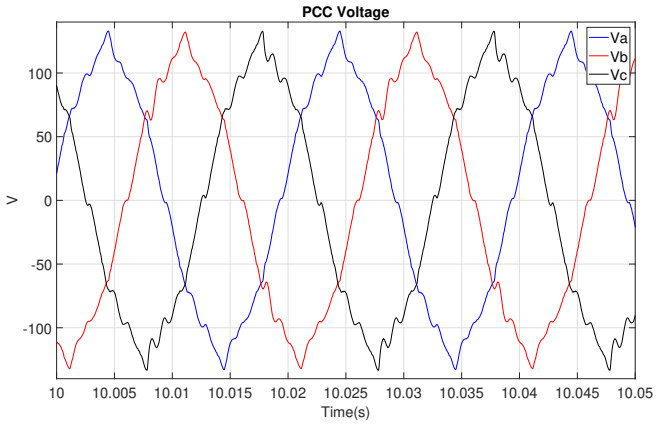

Figure 3.12: Steady state abc voltages after power steps.

The THD here is about 5.5% which is significantly higher than for the weaker grid. Also the peak voltage is about 133 V which is higher than for the strong grid

because higher grid impedance.

3.2.2 Test 2

In this test a negative resistance of 0.25 and a virtual reactance of 3 was added. This gives a reference X/R of 10.5. Figure 3.13shows the active and reactive power delivered to the grid during the test.

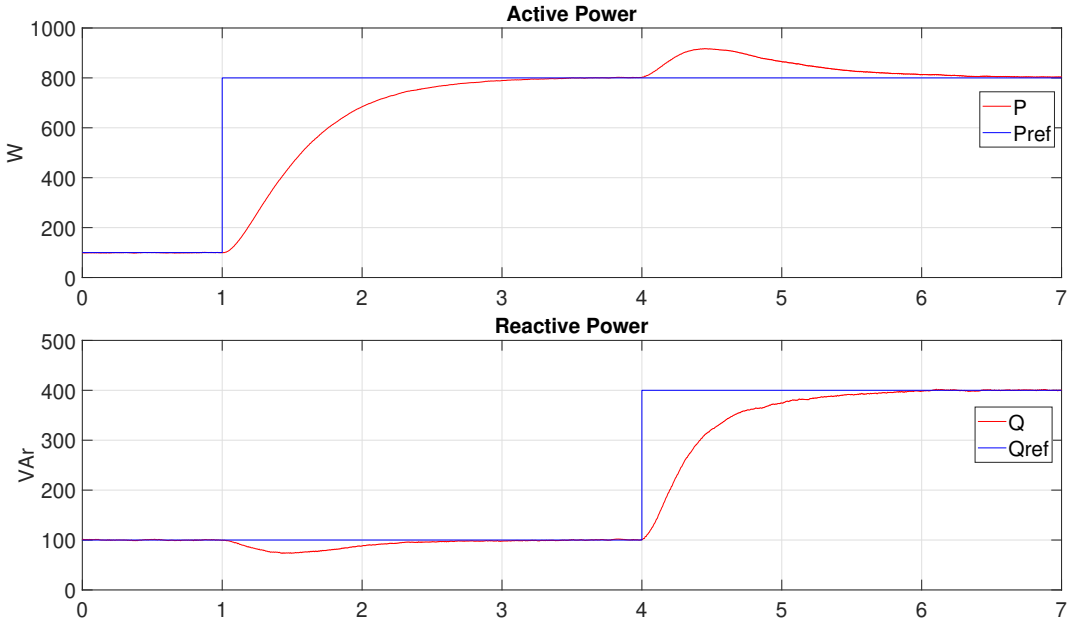

Figure 3.13: Active and Reactive Power Steps Test 2.

In this test the reactive power deviation is 27 VAr which is a significant decrease compared to test 1 with a weak grid and also the test 2 with the strong grid. The active power deviation is 117.7 W which is close to that of test 1 and significantly larger than test 2 for the strong grid. There is no overshoot for the powers and the settling time for the active power is twice as long and for the reactive power it is around 1.5 times as long.

Figure 3.14 shows the estimated resistance, reactance and X/R ratio respectively during the test.

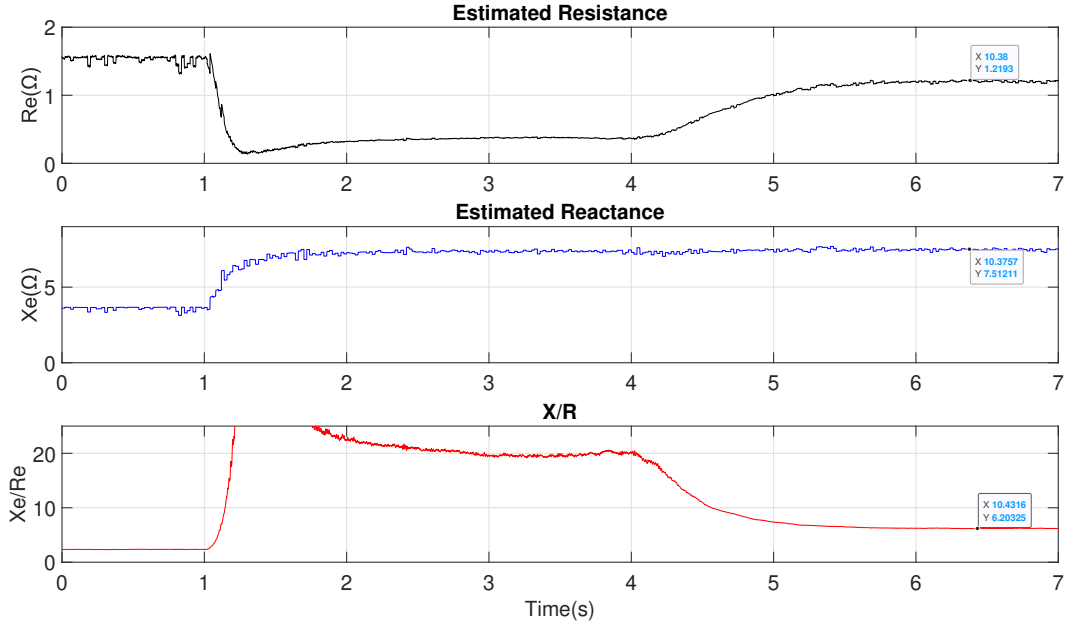

Figure 3.14: The estimated resistance, estimated reactance and estimated X/R ratio for test 2.

Here the estimated X/R is lower than the reference of 10.5. This is because the estimated resistance is around 1.2Ω which is higher than expected.

Figure3.15 shows the steady state abc voltage after both of the power steps have been applied.

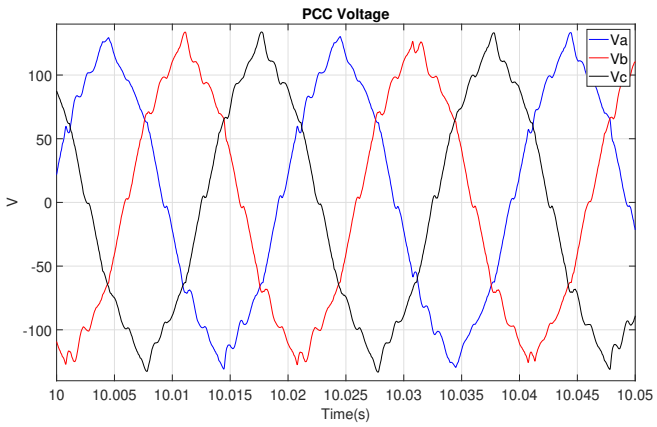

Figure 3.15: Steady state abc voltages after power steps.

The THD is a bit higher than test 1 with 5.75%.

3.2.3 Test 3

In this test a negative resistance of 0.4 and a virtual reactance of 4.15 was added. This gives a reference X/R of 15. Figure 3.16shows the active and reactive power delivered to the grid during the test.

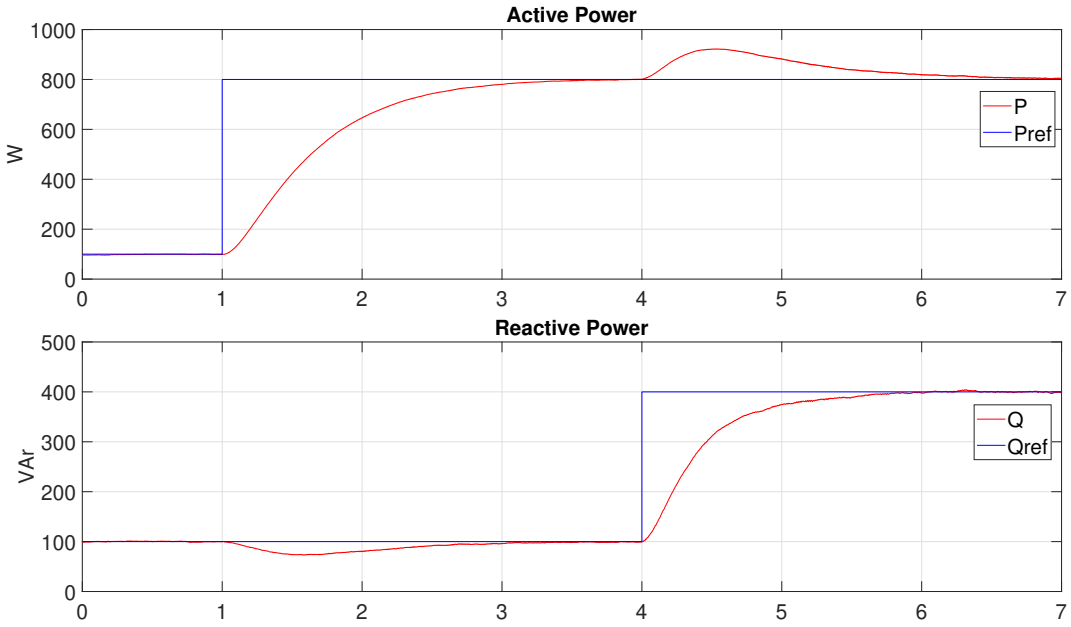

Figure 3.16: Active and Reactive Power Steps Test 3.

Here the reactive power deviation is the same as for test 2. The active power deviation is 122.3 W which is larger than for test 2 and significantly larger than test 3 with the strong grid. The settling time is the longest for all the test for both powers.

Figure 3.17 shows the estimated resistance, reactance and X/R ratio respectively during the test.

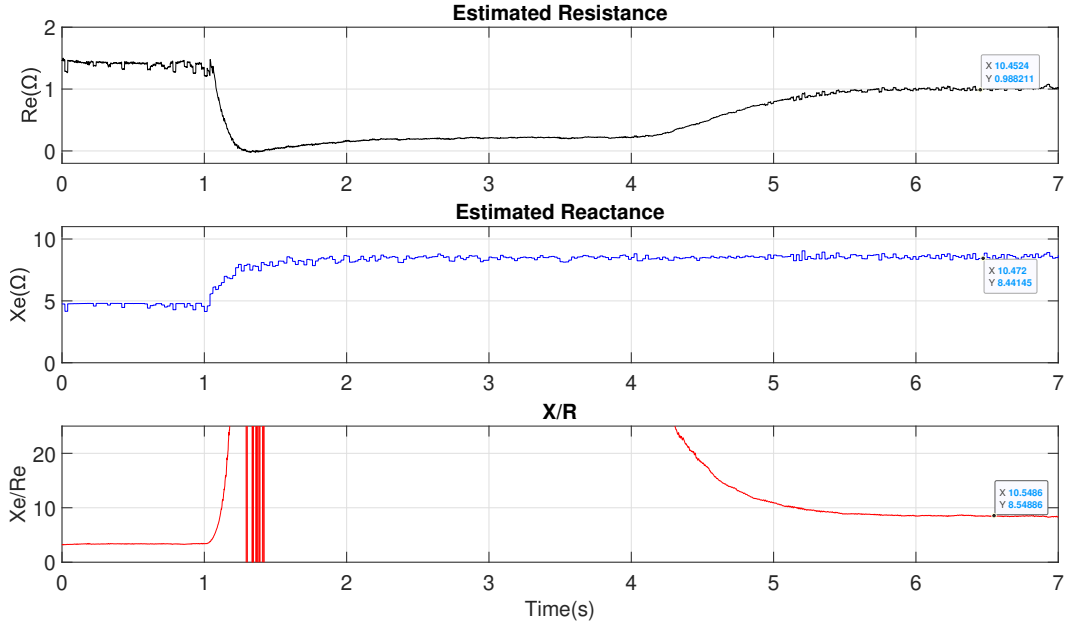

Figure 3.17: The estimated resistance, estimated reactance and estimated X/R ratio for test 3.

As in test 2 the estimated resistance is higher than the reference leading to a lower estimated X/R ratio than the reference.

Figure3.18 shows the steady state abc voltage after both of the power steps have been applied.

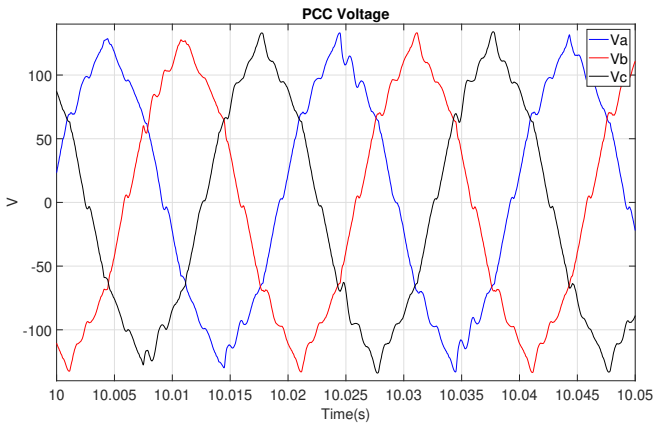

Figure 3.18: Steady state abc voltages after power steps.

Here the THD is 5.8% which is the highest of all test but still withing the grid code limits.

3.3 Comparison

This section shows a comparison of all the results for the different test. These results will be discussed further in Chapter 5.

Table 3.7 compares the active and reactive power response with different X/R ratios and SCR.

Table 3.7: Comparison of the test with different X/R ratios for the strong and weak grid tests.

SCR	Parameter	X/R = 2.83	X/R ≈ 10.5	X/R = 15
13	ΔQ during P Step(VAr)	79.8	41.1	38
	Overshoot P(%)	21.3	8.25	3.5
	Settling Time P Step(s)	0.9	0.845	0.96
	ΔP during Q Step(W)	110.3	67.2	72.8
	Overshoot Q(%)	19.4	9.25	6.6
	Settling Time Q Step(s)	1	0.62	0.78
3	ΔQ during P Step(VAr)	70	27	27
	Overshoot P(%)	1	0	0
	Settling Time P Step(s)	0.92	1.89	2.08
	ΔP during Q Step(W)	123	117.7	122.3
	Overshoot Q(%)	0	0	0
	Settling Time Q Step(s)	1.07	1.56	1.59

Table 3.8 shows the voltage THD of the different tests.

Table 3.8: Voltage THD during steady state after both power steps.

X/R	**THD, SCR=13**	**THD, SCR=3**
2.83	3.3	5.5
10.65	3.5	5.75
15	4	5.8

Chapter 4

Experimental Tests

In this chapter the Simulink model was tested on an experimental set-up. The power grid was emulated by a Cinergia grid emulator. The model was fully discretize and implemented on a dSPACE Simulink set-up in the lab. The set-up had the same grid parameters as in Table 3.3 which is for the strong grid simulation test. Except the grid voltage is 35 Vrms and this leads to a SCR of 6.6. There was no possibilities to change the load to do experimental test with a different SCR. The active power step was 400 W and reactive power step was 200 VAr. The reason for this was complication with the set-up at higher voltage and power. The tests will be examined in the same way as in 3.

4.1 Experimental Set-up and Tests

The Laboratory set-up is shown in Figure 4.1.

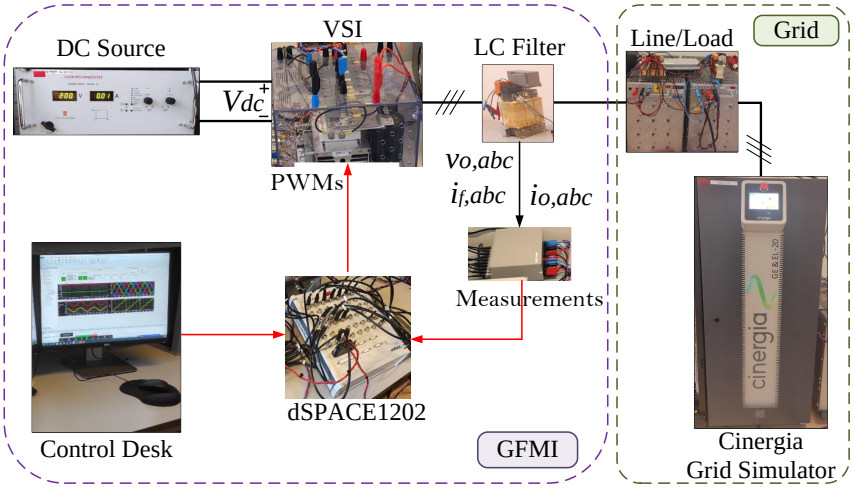

Figure 4.1: Experimental set-up.

Here the VSI is the voltage source inverter and the set-up contains two inductor coils which work as the grid impedance with an inductance of 18 mH and resistance of 0.2Ω each.

The different steps of the experimental tests and when the steps occur can be seen in Table 4.1

Table 4.1: The steps for the experimental test.

Time(s)	Step	**Active Power(W)**	**Reactive Power(VAr)**
0	PLL Synchronisation	0	0
0.45	GFL to GMF Transition	0	0
0.6	Active Power Ramp Up	0-70	0
1	Reactive Power Step	0	0-100
1	Add Virtual Reactance	0	0
1.5	Add Virtual Resistance	0	0
40	Active Power Step	100-500	0
60	Reactive Power Step	0	100-300

Compared to the simulation steps the experimental steps are much further spaced apart and the whole process takes longer.

The gains used in the experimental part were not the same as the simulation as more aggressive proportional gains were needed for a better response.

Table 4.2: PI controller gains for active and reactive controllers.

Parameter	Value
$K_{p,apc}$	0.002005
$K_{i,apc}$	0.0010732
$K_{p,rpc}$	0.00795
$K_{i,rpc}$	0.0795

In Table 4.3 the virtual resistance and impedance added is displayed. These are the same virtual impedance values as Test 1 and 2 in the simulation tests for the strong grid.

Table 4.3: Virtual impedance for experimental tests.

Test	Virtual Resistance(Ω)	Virtual Inductive Reactance(Ω)	X/R ratio
1	0	0	2.83
2	-0.2	1	10.65

4.1.1 Test 1

This test did not have any virtual impedance added and therefore the X/R ratio will be 2.83. Figure 4.2 shows the active and reactive power delivery to the grid during the test.

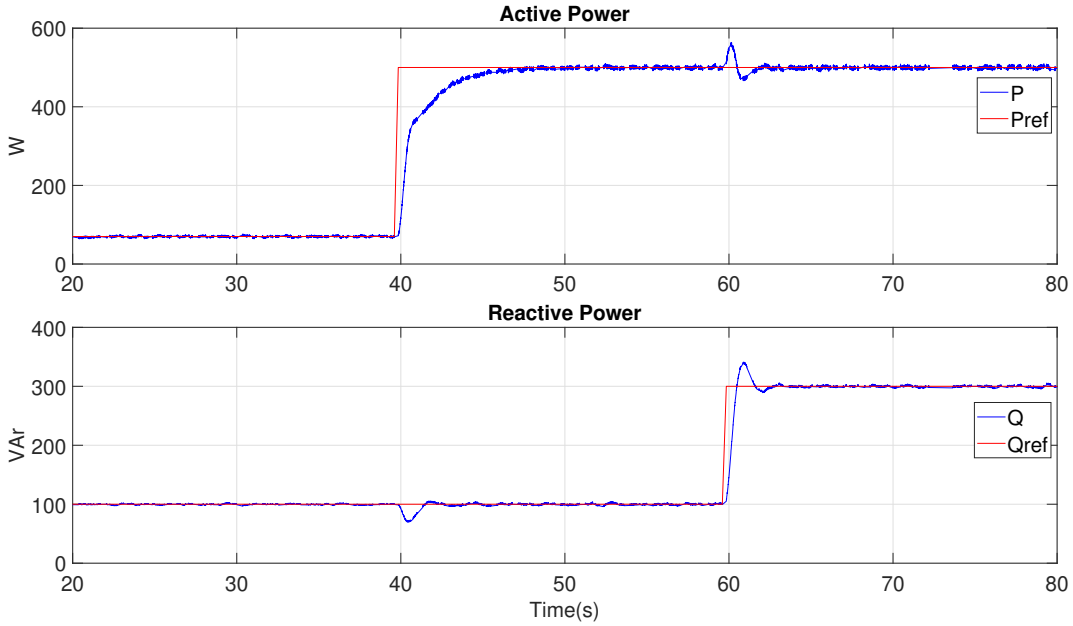

Figure 4.2: Active and reactive power step with no virtual impedance

From the graphs it can be clearly seen that there is coupling between the powers. The reactive power deviates 30.2 VAr and the active power deviated 63.8 W from the reference. This is less of a deviation compared to the simulations with the strong and weak grid for this X/R ratio. In terms of overshoot there is none for the active power and 13.7% for the reactive power. Also the power steps are smaller for the experimental test which can also lead to less deviation. The settling time for the experimental test was 8 seconds for the active power which is a significantly longer than for both simulations tests the same X/R ratio. The reactive power settling time was 2.3 which is also longer than for the simulations.

Figure 4.3 shows the estimated resistance, reactance and X/R ratio.

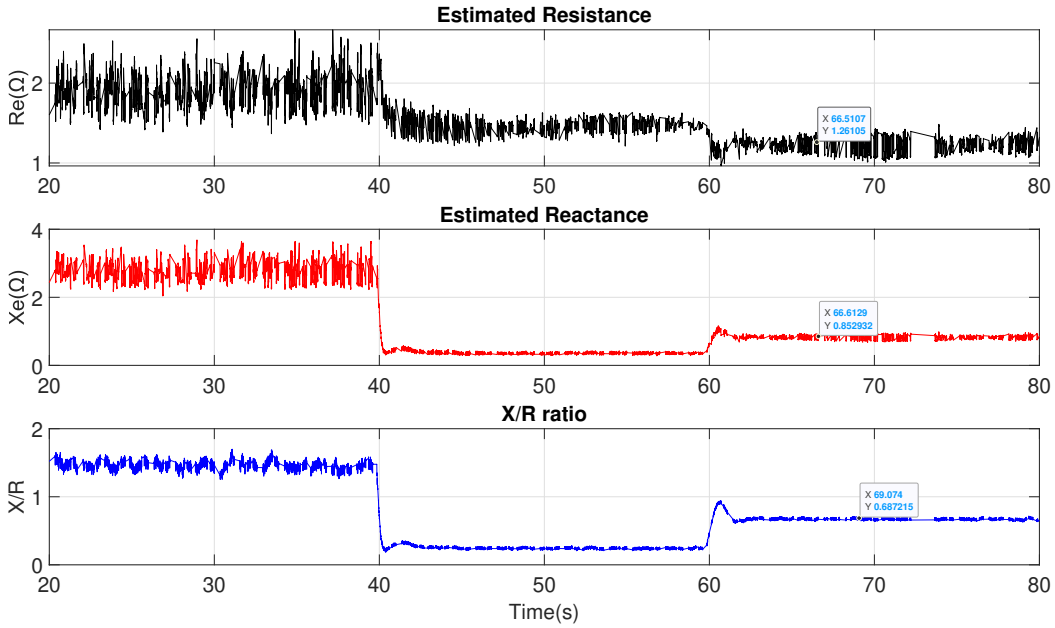

Figure 4.3: X/R ratio with no virtual impedance.

The resistance is here more than 0.6Ω larger than that of the known grid resistance. The reason that this resistance might be higher than for the simulation is the lower voltage and that the simulation does not account for resistance in the equipment. The higher resistance than expected results in a lower X/R ratio of around 0.7.

Figure 4.4 shows the steady state abc voltage after both power steps.

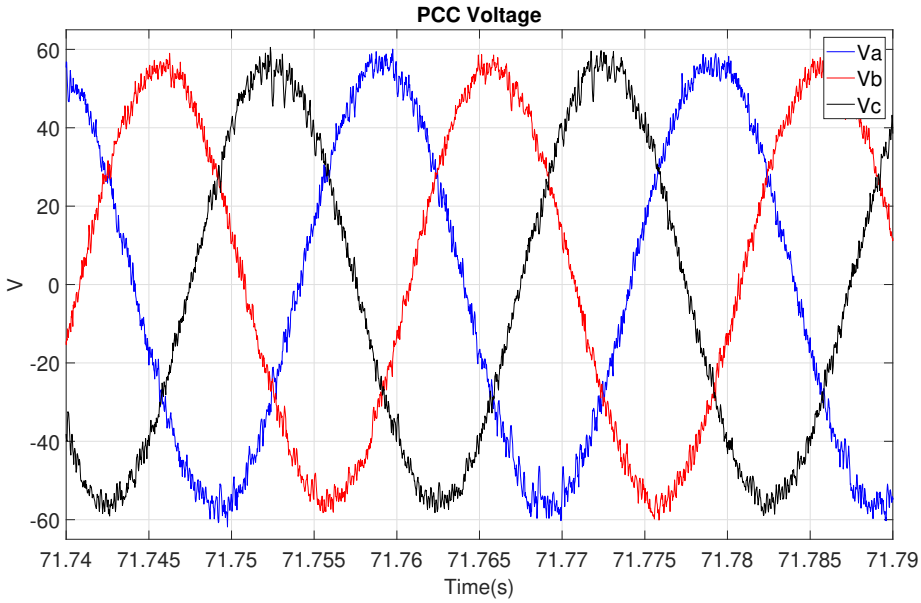

Figure 4.4: abc voltages during steady state with no virtual impedance.

Here the THD is around 4.7 so it is higher than the simulation test%.

4.1.2 Test 2

For this test a negative resistance of 0.2 was added and a virtual reactance of 1. This gives the X/R reference of 10.65. Figure 4.5 shows the active and reactive power during the test delivered to the grid.

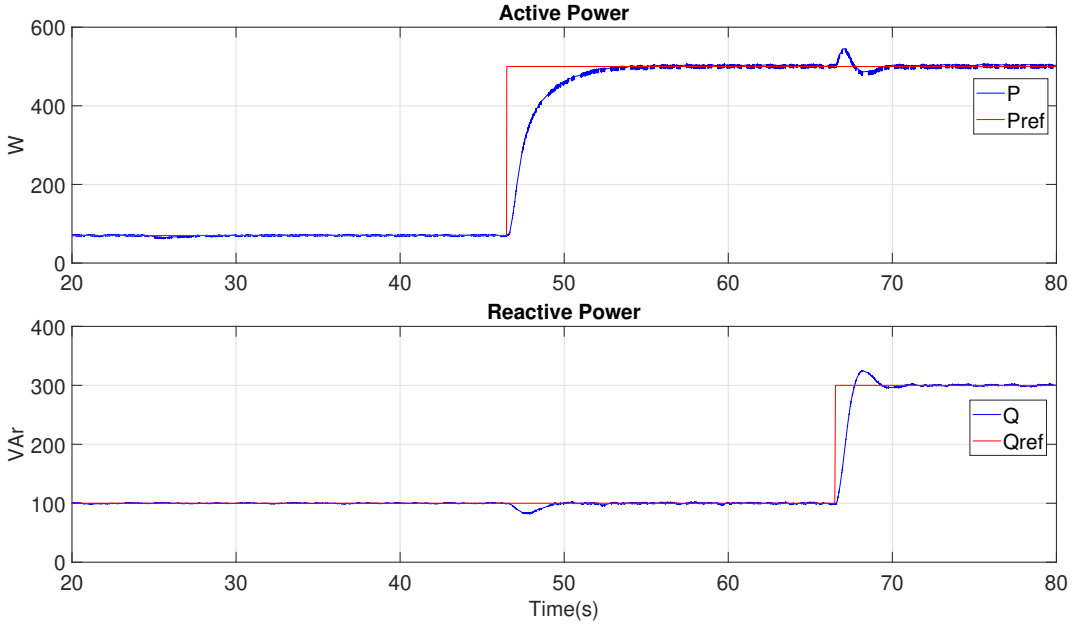

Figure 4.5: Active and reactive power step for test 2 with virtual impedance.

The reactive power deviates 18.1 VAr and the active power deviated 45.2 W from the reference. This is significantly smaller compared to test 1. The settling of the active power is 1.2 seconds shorter compared to test 1 and for the reactive power it is 0.35 seconds longer.

Figure 4.6 shows the estimated resistance, reactance and X/R ratio.

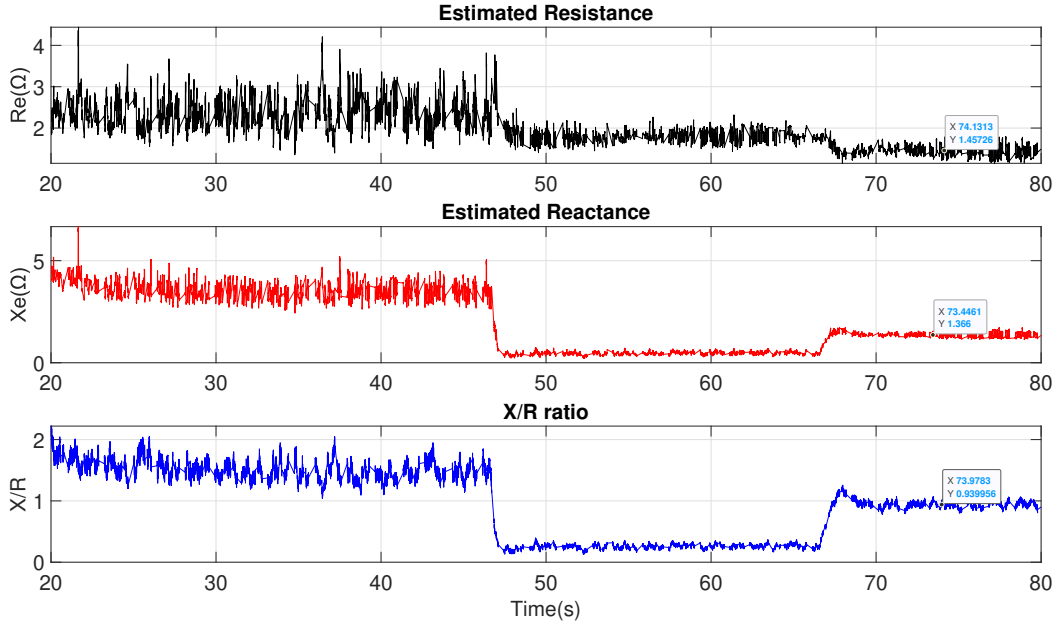

Figure 4.6: Estimated resistance, reactance and X/R ratio with virtual impedance.

Here the X/R ratio only goes to up to around 1 which is far from the reference of 10 but higher than for test 1. The low ratio is mainly due to the high estimated resistance which is around 1.45 after both power steps.

Figure 4.7 shows the steady state abc voltage after both power steps.

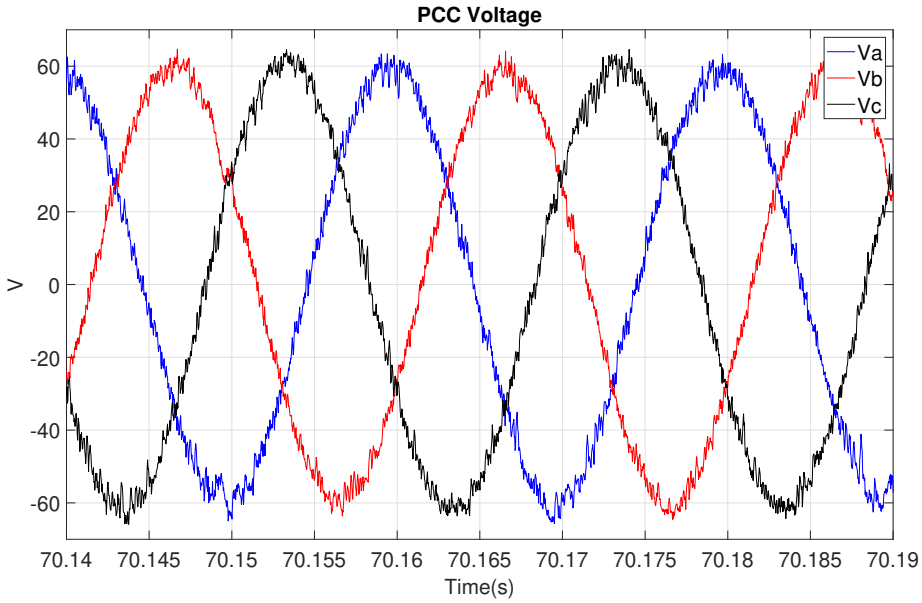

Figure 4.7: abc voltages during steady state with virtual impedance.

THD around 5.5% so it is higher than for test 1 and higher than compared to the simulation test.

4.1.3 Comparison

This section shows a comparison of the experimental results. These results will be discussed further in Chapter 5.

Table 4.4: Comparison of the test with different X/R ratios for the experimental results.

SCR	Parameter	X/R = 2.83	X/R = 10.65
13	ΔQ during P Step(VAr)	30.2	18.1
	Overshoot P(W)	0	0
	Settling Time P Step(s)	8	6.8
	ΔP during Q Step(W)	63.8	45.2
	Overshoot Q(VAr)	13.7	8.5
	Settling Time Q Step(s)	2.3	2.65

Table 4.5 shows the THD of the voltage for both tests.

Table 4.5: THD of the steady state voltage after both power steps.

X/R	**THD**
2.83	4.7
10.65	5.5

Chapter 5

Discussion

The simulation and experimental results both showed clear decoupling between the active and reactive power. This was the case for all the tests expect the tests with the weaker grid during the reactive power step. This was an unexpected result and the because of limited time to figure out the reason for this, an explanation for this will not be discussed.

When it comes to the exact effect of the virtual impedance on the X/R ratio there is an uncertainty. The EGIE did not always give good estimations, it did however give some rough estimates after both power steps were done. For example the strong grid had a X/R ratio of 2.83 and The EGIE showed a X/R ratio of around 8 after the active power step and 4.2 after the reactive power step. This means that the impedance estimations when adding virtual impedance can not be certain. Also the EGIE in the simulations showed higher X/R ratios for the strong grid and lower for the weak grid. For the experiments it showed a significantly lower X/R ratio than expected.

However the simulation results for the strong grid showed there was a significant decoupling when going from a desired X/R ratio of 2.83 to 10.65 for both active and reactive power. The difference between a ratio of 10 and 15 was not as significant in terms of decoupling. It is important to note that there was a significantly larger overshoot for the X/R ratio of 2.83 compared the other ratios. This could have lead to a higher deviation because the active power went higher. However there was still a clear decoupling as the deviation from the reference decreased significantly.

For the the weaker grid during the active power step there was also significant decoupling between X/R of 2.83 and 10.65, even more than for the strong grid.

A reason that going from 2.83 to 10.65 in X/R ratio decouple more than going from 10.6 to 15 can be because the feeder impedance goes from resistive to inductive. The results shows that there is not a significant benefit in terms of decoupling

to increase the X/R more than 10.65 where the line becomes inductive.

For the experimental tests there was only two X/R ratios tested. The coupling halved during the active power step when increasing the desired X/R ratio from 2.83 to 10.6. The decoupling during the reactive power step was not as significant but still there was a clear decoupling. The EGIE however showed higher resistance and lower reactance than that of the desired value. These values were far from the rough estimates seen in the simulation results. This can mean that there is an extra resistance coming from a connection between the grid simulator and inverter. The lower reactance is not certain but can possibly come from the lower voltage. When adding the virtual impedance the EGIE did not give estimated values close to the desired ones.

Comparing the step responses for all simulation tests there was a clear damping factor from virtual impedance. In theory grid impedance lead to damping and from these results it can be seen that virtual impedance has a similar effect. The weaker grid had a higher line impedance therefore there was more damping in the system and the responses was slower compared to the strong grid. For the experimental test however there was not a damping effect on the active power when adding virtual impedance. Here the step response became less damped it seemed. For the reactive power it became more damped however.

The experimental test for the active power step was significantly slower than for both simulations and the reactive power step was also slower. This is most likely due to the the low voltage which as seen in Equations 2.9 and 2.13 plays a role on the transfer function. For the active power the voltage is the grid voltage squared and this could lead to the much slower response.

The voltage for the weak grid was higher during the reactive power step to compensate for the higher grid impedance. The THD of the abc voltage also increased for the weak grid. Adding virtual impedance also increased the THD. For the experimental tests the THD was a bit lower than for the weak grid. All the tests were within the IEEE standard THD limits.

5.1 Future Work

The first thing that would be beneficial for this project is to do the experimental tests with the same voltage and the same SCR of the simulation tests. Also the X/R ratios of 15 would be interesting to test experimentally.

Also it would be interesting to do more tests to try to figure out why the active power did not decouple when adding virtual impedance for the weak grid.

The EGIE could also be improved so the virtual impedance could be controlled

by a closed loop VI-PR. This would mean that the GFM inverter could decouple the power without knowing the grid impedance and for varying impedance. There would have to be a limit for how much the ratio could change before a new virtual impedance reference would be added. Within this limit a fine tuning algorithm would be used to give a needed virtual reactance to stabilize the X/R ratio. This fine tuning method could be a sliding mode controller like in [3] or artificial neural network method used in [10], which would be a new fine tuning method for GFM inverters.

Chapter 6

Conclusion

This thesis focused on decoupling active and reactive power for a GFM inverter by adding virtual impedance to increase the X/R ratio. This method has been tested through simulations and experimental tests. Three different X/R ratios were tested for both a strong and a weaker grid though simulations, also tests for a strong grid was tested experimentally.

From the tests it can be concluded that there is a clear decoupling between both the active and reactive power when adding virtual impedance for a strong grid. The weaker grid test showed clear decoupling during a active power step but not during a reactive power step. Due to lack of time this unexpected effect was not investigated further.

Also adding a virtual impedance to get a desired X/R ratio of 15 did not give significant decoupling compared to X/R ratio of 10.6. Adding virtual impedance also showed clear effect on the step response of the system, as it gave a damping effect.

For the experimental tests the settling time was much longer especially for the active power. This is most likely due to the voltage being halved, due to the complications during higher voltage.

Bibliography

[1] Dayan B. Rathnayake et al. "Grid Forming Inverter Modeling, Control, and Applications". eng. In: *IEEE access* 9 (2021), pp. 114781–114807. ISSN: 2169-3536.

[2] Frede Blaabjerg. *Control of power electronic converters and systems. Volume 3*. eng. London, England: Academic Press, 2021. ISBN: 0-12-819433-2.

[3] Ricardo Lucio De Araujo Ribeiro et al. "Adaptive Grid Impedance Shaping Approach Applied for Grid-Forming Power Converters". eng. In: (2022). ISSN: 21693536.

[4] Donghua Pan et al. "Transient Stability of Voltage-Source Converters With Grid-Forming Control : A Design-Oriented Study". eng. In: (2020). ISSN: 21686777.

[5] Usman Bashir Tayab et al. "A review of droop control techniques for microgrid". In: *Renewable and Sustainable Energy Reviews* 76 (2017), pp. 717–727. ISSN: 1364-0321. DOI: https://doi.org/10.1016/j.rser.2017.03.028. URL: https://www.sciencedirect.com/science/article/pii/S1364032117303453.

[6] Haiya Qian et al. "Analysis and implementation of virtual impedance for fixed-frequency control strategy in microgrid". eng. In: *IET generation, transmission distribution* 15.15 (2021), pp. 2262–2276. ISSN: 1751-8687.

[7] Lin Yu et al. "A Critical System Strength Evaluation of a Power System with High Penetration of Renewable Energy Generations". eng. In: *CSEE Journal of Power and Energy Systems* 8.3 (2022), pp. 710–720. ISSN: 2096-0042.

[8] Xian Gao et al. "A Comparative Study of Grid-Following and Grid-Forming Control Schemes in Power Electronic-Based Power Systems". eng. In: (2023). ISSN: 25434292.

[9] Arman Oshnoei and Frede Blaabjerg. *Sliding Mode-based Model Predictive Control of Grid-Forming Power Converters*. eng. 2023.

[10] Tomislav Dragicevic and Mateja Novak. “Weighting Factor Design in Model Predictive Control of Power Electronic Converters : An Artificial Neural Network Approach”. eng. In: (2019). ISSN: 02780046.

[11] ENERGINET. *Tilslutning af produktionsanlæg til transmissionsnettet Requirements for Generators(RfG)*. https://energinet.dk/media/mnqiqxih/vejledning-rfg_tilslutning-af-produktionsanlg-til-transmissionsnettet-revision-1-juni-2021.pdf. Seen: 19-12-2023. 2021.

[12] N. Cho, B. Wendha, and M. Luthfi. “Evaluations on the harmonic allocation methods of IEC 61000-3-6 and IEEE Standard 519 in the distribution systems”. In: *Electric Power Systems Research* 230 (2024), p. 110260. ISSN: 0378-7796. DOI: https://doi.org/10.1016/j.epsr.2024.110260. URL: https://www.sciencedirect.com/science/article/pii/S0378779624001482.

[13] Arman Oshnoei et al. *Grid synchronization for distributed generations*. eng. 2023.

Appendix A

Phase Locked Loop

For GFL inverters to synchronizing to the grid a phase locked loop(PLL) is needed[2]. Also GFM inverters usually use a PLL to initially synchronize to the grid. In this project a synchronous reference frame PLL(SRF-PLL) is used. This method is used for three phase systems. By using reference frame transformations the three phase voltage can be transferred into the dq frame. The q-axis voltage is then used as the reference. When the q-axis voltage is zero the voltage will be synchronized. Figure A shows the SRF-PLL.

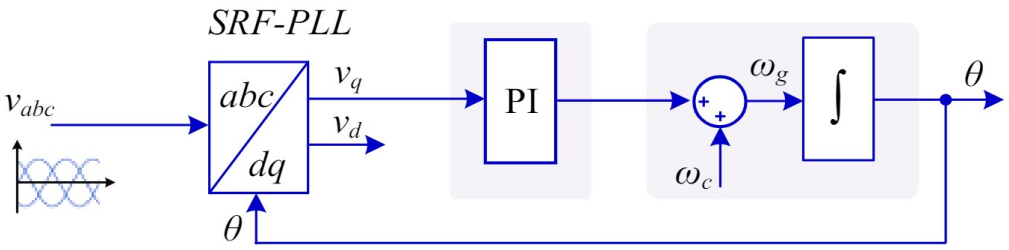

Figure A.1: Block di[13]

Here a PI controller is used to correct the Vq voltage by first giving a reference frequency which is added by the reference frequency. This is then integrated to get the phase angle needed to synchronize.